

**AFRL-SN-RS-TR-2001-185**  
**In-House Technical Report**  
**September 2001**



## **KNOWLEDGE-BASE APPLICATION TO GROUND MOVING TARGET DETECTION**

**R. Adve, P. Antonik, W. Baldygo, C. Capraro, G. Capraro, T. Hale, R. Schneible,  
and M. Wicks**

*APPROVED FOR PUBLIC RELEASE; DISTRIBUTION UNLIMITED.*

**AIR FORCE RESEARCH LABORATORY  
SENSORS DIRECTORATE  
ROME RESEARCH SITE  
ROME, NEW YORK**

**20011109 070**

This report has been reviewed by the Air Force Research Laboratory, Information Directorate, Public Affairs Office (IFOIPA) and is releasable to the National Technical Information Service (NTIS). At NTIS it will be releasable to the general public, including foreign nations.

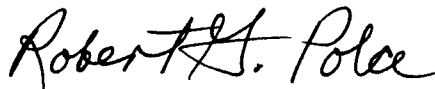
AFRL-SN-RS-TR-2001-185 has been reviewed and is approved for publication.

APPROVED:



GERARD J. GENELLO, Branch Chief  
Radar Signal Processing Branch

FOR THE DIRECTOR:



ROBERT G. POLCE, Chief  
Rome Operations Office  
Sensors Directorate

If your address has changed or if you wish to be removed from the Air Force Research Laboratory Rome Research Site mailing list, or if the addressee is no longer employed by your organization, please notify AFRL/SNRT, 26 Electronic Pky, Rome, NY 13441-4514. This will assist us in maintaining a current mailing list.

Do not return copies of this report unless contractual obligations or notices on a specific document require that it be returned.

REPORT DOCUMENTATION PAGE			Form Approved OMB No. 0704-0188	
<small>Public reporting burden for this collection of information is estimated to average 1 hour per response, including the time for reviewing instructions, searching existing data sources, gathering and maintaining the data needed, and completing and reviewing the collection of information. Send comments regarding this burden estimate or any other aspect of this collection of information, including suggestions for reducing this burden, to Washington Headquarters Services, Directorate for Information Operations and Reports, 1215 Jefferson Davis Highway, Suite 1204, Arlington, VA 22202-4302, and to the Office of Management and Budget, Paperwork Reduction Project (0704-0188), Washington, DC 20503.</small>				
1. AGENCY USE ONLY (Leave blank)		2. REPORT DATE SEPTEMBER 2001		3. REPORT TYPE AND DATES COVERED In-House 1997-2000
4. TITLE AND SUBTITLE KNOWLEDGE -BASE APPLICATIONS TO GROUND MOVING TARGET DETECTION			5. FUNDING NUMBERS PE - 62204F PR - 762R TA - PR WU - OJ	
6. AUTHOR(S) R. Adve, P. Antonik, W. Baldygo, C. Capraro, G. Capraro, T. Hale, R. Schneible, M. Wicks				
7. PERFORMING ORGANIZATION NAME(S) AND ADDRESS(ES) AFRL/SNRT 26 Electronic Pky Rome NY 13441-4514			8. PERFORMING ORGANIZATION REPORT NUMBER  AFRL-SN-RS-TR-2001-185	
9. SPONSORING/MONITORING AGENCY NAME(S) AND ADDRESS(ES) AFRL/SNRT 26 Electronic Pky Rome NY 13441-4514			10. SPONSORING/MONITORING AGENCY REPORT NUMBER  AFRL-SN-RS-TR-2001-185	
11. SUPPLEMENTARY NOTES  Air Force Research Laboratory Project Engineer: Michael C. Wicks, SNRT, 315-330-2556				
12a. DISTRIBUTION AVAILABILITY STATEMENT Approved for public release: distribution unlimited			12b. DISTRIBUTION CODE	
13. ABSTRACT (Maximum 200 words)  This report summarizes a multi-year in-house effort to apply knowledge-base control techniques and advanced Space-Time Adaptive Processing algorithms to improve detection performance and false alarm control in Ground Moving Target Indication Airborne Radar.				
14. SUBJECT TERMS Radar, algorithms, signal processing, space-time adaptive processing			15. NUMBER OF PAGES 104	
			16. PRICE CODE	
17. SECURITY CLASSIFICATION OF REPORT  UNCLASSIFIED	18. SECURITY CLASSIFICATION OF THIS PAGE  UNCLASSIFIED	19. SECURITY CLASSIFICATION OF ABSTRACT  UNCLASSIFIED	20. LIMITATION OF ABSTRACT  UL	

# Table of Contents

List of Figures	ii
List of Tables	iii
Executive Summary	1
1.0 Introduction: Why STAP for GMTI?	3
2.0 Background	5
2.1 <i>Sigma-Delta STAP</i>	9
2.1.1 $\Sigma\Delta$ -STAP Algorithm Development	10
2.1.2 Numerical Example	12
2.1.3 Discussions: Advantages and Limitations	13
2.2 <i>Joint Domain Localized Processing in the Ideal Case</i>	15
2.3 <i>JDL Processing Accounting for Array Effects</i>	18
2.3.1 Multi-Channel Airborne Radar Measurements (MCARM)	20
2.3.2 Example 1: Injected target	23
2.3.3 Example 2: MTS Tones	24
2.4 <i>Non-Homogeneity Detection/Knowledge Based Processing</i>	26
2.5 <i>Direct Least Squares Approach</i>	28
2.5.1 Performance of $D^3$ Processing in Non-homogeneous Interference	32
3.0 Advances in GMTI-STAP	35
3.1 <i>Hybrid (<math>D^3</math>/JDL) STAP- A GMTI Specific Algorithm</i>	35
3.1.1 Two-Stage Hybrid Algorithm	36
3.1.2 Example 1: Simulated Data	38
3.1.3 Applying the Hybrid Algorithm to Measured Data	40
3.1.4 Example 2: Injected Target in MCARM Data	41
3.1.5 Example 3: MTS Tones in the MCARM Data:	43
3.1.6 Summary	45
3.2 <i>Knowledge Based Processing</i>	46
3.3 <i>MAP-STAP</i>	51
3.3.1 Representative Secondary Clutter Data	53
3.3.2 A Priori Information	54
3.3.3 Research Problem, Hypothesis, and Preliminary Findings	55
3.3.4 Discussion	61
4.0 GMTI STAP Future Work	61
4.1 $D^3 \Sigma\Delta$ STAP	61
4.2 <i>Additional Algorithms</i>	63
4.2.1 Evolutionary Algorithms	63
5.0 Roadmap to the Future	64
6.0 References	67

## List of Figures

Figure 1: Performance Comparison of Airborne Array Radar Signal Processing Techniques	3
Figure 2: Performance Loss Due to the Velocity-PRI Constraint on Target Detection	4
Figure 3: GMTI-STAP Goal	4
Figure 4 : Angle-Doppler structure of clutter	5
Figure 5 : Estimating the space-time interference covariance matrix	6
Figure 6: Clutter Non-Homogeneity	7
Figure 7: Past and Proposed STAP efforts	8
Figure 8: Block Diagram of general $\Sigma\Delta$ -STAP	10
Figure 9: Performance of $\Sigma\Delta$ -STAP compared to Pulse Doppler processing	13
Figure 10: Linear Array of Point Sensors	15
Figure 11: Localized Processing Regions in JDL for $\eta_a - \eta_d = 3$	17
Figure 12: MCARM Testbed	21
Figure 13: MCARM Antenna Array	21
Figure 14: Magnitude of MCARM steering vectors	22
Figure 15: JDL performance before and after accounting for array effects (Injected Target)	24
Figure 16: JDL before and after accounting for array effects (MTS Tones)	25
Figure 17: Secondary Data Selection (a) Homogeneous Case (b) Non-homogeneous Case	26
Figure 18: Non-Homogeneity Detection in LPR and in Factored Approaches	28
Figure 19: Principle of Direct Data Domain Processing	29
Figure 20: JDL Antenna Patterns at Target Doppler and Azimuth	33
Figure 21: Direct Data Domain Patterns at Target Doppler and Azimuth	34
Figure 22: Block diagram of the Two-Stage Hybrid Algorithm	36
Figure 23: Three $D^3$ spatial beams used to form LPR	38
Figure 24: Hybrid Algorithm Patterns at Target Doppler and Azimuth	39
Figure 25: Performance of Hybrid algorithm in countering non-homogeneities: Injected Target (a) With Non-homogeneity, No target (b) With non-homogeneity, With target	42
Figure 26: Performance of Hybrid algorithm in countering non-homogeneities: MTS Data (a) With Non-homogeneity, No target (b) With non-homogeneity, With target	44
Figure 27: Beam Pattern associated with the Hybrid and JDL methods	45
Figure 28: Knowledge Based Space-Time Adaptive Processing (KB-STAP)	46
Figure 29: Location and transmit direction of the MCARM Aircraft during the acquisition	48
Figure 30 : JDL Processing without accounting for non-homogeneities	49
Figure 31: Combined processing accounting for non-homogeneities	50
Figure 32: Sources of Information for KB-STAP	52
Figure 33: Range Ring and Doppler Patch Model with Constant Frequency Hyperbola	53
Figure 34: Radar Visualization of Terrain Clutter and Injected Targets	56
Figure 35: MSMI Output With No Injected Target	57
Figure 36: MSMI Output With Injected Target at Range Bin 475	58
Figure 37: MSMI Output With Injected Target At Range Bin 375	59
Figure 38: MSMI Output With Injected Target At Range Bin 296	60
Figure 39: Sum and Difference $D^3$ Beam Patterns	62
Figure 40: GMTI STAP Plan	64
Figure 41: Technology Program Roadmap	65
Figure 42: Technology Maturation Program Roadmap	65
Figure 43: GMTI STAP Program Roadmap	66

## **List of Tables**

Table 1: Parameters for example using simulated data	32
Table 2: Parameters for injected non-homogeneity and target in MCARM Data	41
Table 3: Parameters of the injected targets	48

## **ACKNOWLEDGEMENTS**

The authors wish to thank Mr. Gerard Genello, Jr. from AFRL/SNRT Radar Signal Processing Branch, and Dr. Joseph Guerri from DARPA for their interest and support.

Technical contributors to this report include: R. Adve, P. Antonik, W. Baldygo, C. Capraro, G. Capraro, T. Hale, R. Schneible, and M. Wicks. Typing and Graphics Support was provided by P. Woodard.

## Executive Summary

The major impact of the research reported herein is the development of an adaptive algorithm that specifically addresses the rejection of discretes in the cell under test competing with all targets; and the rejection of distributed clutter competing with slow moving targets. Discretes can include large fixed clutter returns and multiple moving objects in the sidelobes.

This report discusses the development of space-time adaptive processing (STAP) technology for ground moving target indication (GMTI) applications. Current GMTI systems, e.g. the E-8 Joint STARS, use non-adaptive displaced phase center antenna (DPCA) techniques. The Joint STARS platform has been very successful in certain deployments, such as the Gulf War. So the question naturally arises, why is STAP needed for GMTI?

In theory, DPCA can outperform some (suboptimal) STAP implementations. DPCA may also perform better in highly non-homogeneous environments, where sufficient training data for adaptive systems is not available. However, when hardware and system errors are considered, the performance of DPCA degrades rapidly. For example, phase, and amplitude errors between channels impose a fundamental limit on non-adaptive DPCA processing. Adaptive processing is several orders of magnitude less sensitive to receiver channel errors.

STAP has demonstrated much better clutter rejection than DPCA for high velocity targets. This is because an adaptive null placed in the sidelobe region by STAP is significantly lower than the error sidelobes that limit DPCA performance. On the other hand, DPCA has traditionally provided better performance in the low velocity region, which corresponds to the main beam clutter. The objective of this research is to extend the advantages of STAP in the high velocity region to lower velocity targets. This requires some fundamental re-design of the STAP process. Merely executing the current suite of STAP algorithms in the low-velocity region is inadequate.

This report summarizes past, present and proposed future STAP research at the Air Force Research Laboratory, Radar Signal Processing Branch. The theme of this research has been to move from AMTI STAP theory to GMTI STAP for real systems. STAP algorithms were developed under several simplifying assumptions. The adaptive weights are determined statistically, based on an estimated interference covariance matrix. This estimation requires a large number of homogeneous data samples, i.e. sample support. In the real world, the received data is non-homogeneous, and the required sample support is not available. Special techniques must be developed to counter spatially non-homogeneous interference. In addition, STAP techniques ignore array electromagnetic effects. This issue is of importance in applying STAP to real arrays.

The research presented here has addressed the issues of sample support and array effects. The sample support required is directly proportional to the number of adaptive weights to be determined. This report presents two algorithms,  $\Sigma\Delta$  STAP and Joint Domain Localized (JDL) Processing, that yield excellent interference suppression with a limited number of unknowns. Array effects are addressed for the JDL algorithm through the use of spatial steering vectors that account for array mutual coupling. Using measured data, the examples present significant performance improvements by accounting for array effects. For non-homogeneous scenarios, we present an alternative Direct Data Domain ( $D^3$ ) processing approach.  $D^3$  algorithms do not estimate a covariance matrix and provide effective suppression of discrete interference.  $D^3$  algorithms do not provide as effective suppression of spatially correlated interference as compared to covariance matrix based techniques.

In non-homogeneous interference, researchers have used a non-homogeneity detector (NHD) to identify the non-homogeneous regions of the radar scene. The radar data cube is divided into homogeneous and non-homogeneous range cells. Traditional STAP may be applied within the homogeneous cells, though only using homogeneous cells for sample support. However, by definition of statistical algorithms, traditional STAP cannot suppress the non-homogeneous component of interference. This report presents the hybrid algorithm, a combination of  $D^3$  processing and JDL with the benefits of both. The hybrid algorithm provides effective suppression of both discrete and spatially correlated interference. This algorithm is a significant achievement because it (1) rejects discrete clutter in the test cell against which covariance matrix approaches are totally ineffective and (2) outperforms the  $D^3$  by 30dB against distributed mainlobe clutter. This performance combination is unique in STAP.

The sum total of thirty years of research into STAP is that no single algorithm is optimal in all interference scenarios. Our ongoing research moves towards the Knowledge Based STAP (KB-STAP) concept where the adaptive algorithm and its associated training is chosen "intelligently" to best detect weak and slow moving targets. Here we present the use of terrain maps to determine the sample support for the adaptive process. The use of maps allows the adaptive process to choose the best representative sample support to estimate the clutter covariance matrix. This approach is a first step to the development of practical KB-STAP.



## 1.0 Introduction: Why STAP for GMTI?

Airborne surveillance radar systems operate in a severe and dynamic interference environment. The interference is a sum of clutter, other moving objects, possible deliberate electronic counter measures (ECM) and noise. The ability to detect weak airborne and ground targets requires the suppression of interference in real time. Space-Time Adaptive Processing (STAP) techniques promise to be the best means to suppress such interference.

This report summarizes past, present and proposed future STAP research efforts at the Air Force Research Laboratory, Radar Signal Processing Branch (AFRL RRS). Recently AFRL RRS has focused on STAP as applied to the Ground Moving Target Indication (GMTI) problem. This is an on-going effort and this report details the initial efforts in this area.

The processing technique presently employed for GMTI systems is displaced phase center antenna (DPCA). In DPCA the Doppler spectrum of the sidelobe clutter is folded into the mainlobe and centered at zero Doppler, thus minimizing the spread induced by platform motion. Theoretically, in benign interference environments, this technique can outperform advanced adaptive techniques (Figure 1) [1].

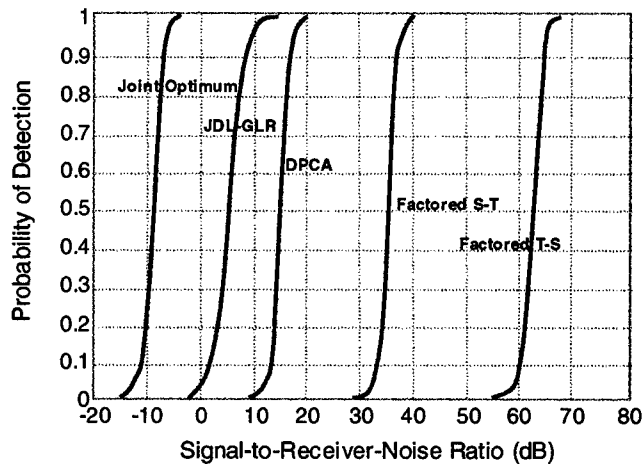


**Figure 1: Performance Comparison of Airborne Array Radar Signal Processing Techniques**

In practice, however, there are several factors that limit the performance of DPCA. System errors, such as the channel-to-channel mismatch, are the prime limiting factor. In addition, DPCA processing is heavily dependent on an assumed relationship between platform velocity and the radar PRI. Deviation from this relationship leads to severely degraded performance (Figure 2). Furthermore, at any time only a fraction of the array channels is used, i.e. DPCA uses the antenna aperture inefficiently.

In contrast to DPCA, STAP uses the multiple channel receive data vector to determine where to place nulls: spatial nulls for point interference, such as jammers and space-time nulls for extended interference, such as clutter. STAP is therefore effective

against all forms of interference, both unintentional and intentional ECM. Furthermore, STAP is much less sensitive (by orders of magnitude) to receiver channel errors.

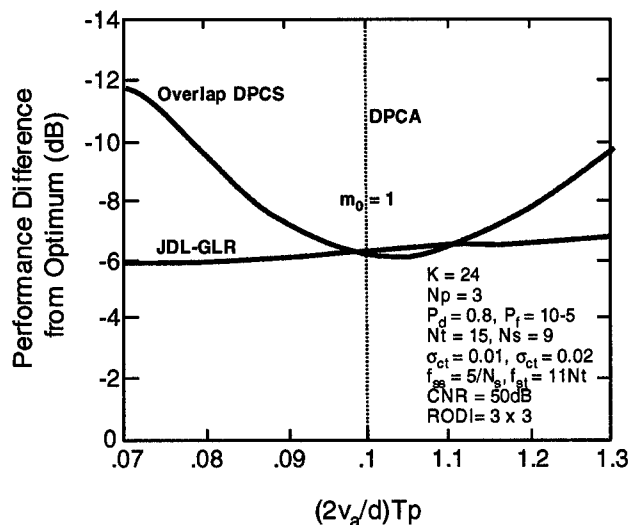


Figure 2: Performance Loss Due to the Velocity-PRI Constraint on Target Detection

For an accurate comparison between processing approaches, hardware errors of actual radars must be considered. Phase and amplitude errors in the multiple channels of the DPCA system impose a basic limit on non-adaptive DPCA processing. On the other hand, STAP is limited by channel mismatch across bandwidth and by processor hardware effects, such as quantization. Traditionally, STAP has been applied to the AMTI mission wherein the high velocity airborne targets are offset from mainbeam clutter in Doppler. For high velocity targets, STAP has demonstrated much better interference rejection than can be obtained with DPCA. This is because STAP can place an adaptive null in the sidelobe region that is significantly lower than the error sidelobes that limit DPCA. The location, depth and width of the null can be determined adaptively based on the interference to be suppressed.

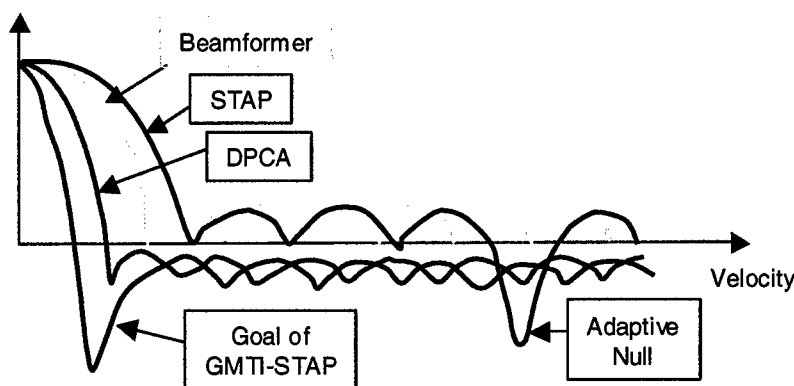


Figure 3: GMTI-STAP Goal

Extensive research into STAP for the AMTI mission, i.e. high radial velocity targets competing with clutter from the antenna sidelobes, has proven its superiority over current non-adaptive processing techniques. Looking to the future, the advantages of STAP for the AMTI mission needs to be extended to the GMTI mission, i.e. slow targets competing with clutter from the antenna mainlobe (Figure 3). This report discusses the approach and progress in that area.

The theme of this report is to present the transition of space-time adaptive processing from AMTI as developed in theory to GMTI in practice. This report presents past, on-going and proposed research to support this transition to practical *knowledge-based adaptive processing* for GMTI. Section 1.0 presents a review of STAP and the issues to be addressed to field STAP. In particular, Section 2.0 presents the concepts of reduced degrees of freedom (DOF), array effects and non-homogeneous interference scenarios. The algorithms and concepts presented in this section represent past work at AFRL. Section 3.0 presents on-going work in STAP, supported by DARPA, including the new hybrid algorithm and MAP-STAP. These concepts are developed in support of the Knowledge-Based STAP concept (KB-STAP) as applied to the GMTI problem. Section 4.0 presents proposed research enhancing STAP for the GMTI mission. Both planned near-term activity and possible far-term efforts are discussed.

In this report, italicized letters denote scalars and integers, such as  $x$  and  $N$ , and lower case bold italic characters denote column vectors, e.g.  $\mathbf{x}$ . Upper case bold italic characters such as  $\mathbf{R}$  denote matrices, while subscripts to bold characters represent the entries in the vector or matrix, such as  $\mathbf{R}_{nm}$ . A superscript  $T$  denotes the transpose and the superscript  $H$  denotes the Hermitian transpose of a vector or matrix.

## 2.0 Background

The goal of adaptive processing is to weight the received space-time data vectors to maximize the output signal-to-interference plus noise ratio (SINR). Traditionally, the weights are determined based on an estimated covariance matrix of the interference. The weights maximize the gain in the look direction, while placing pattern nulls in the interference directions. This interference plus noise is a combination of clutter, ECM and thermal noise.

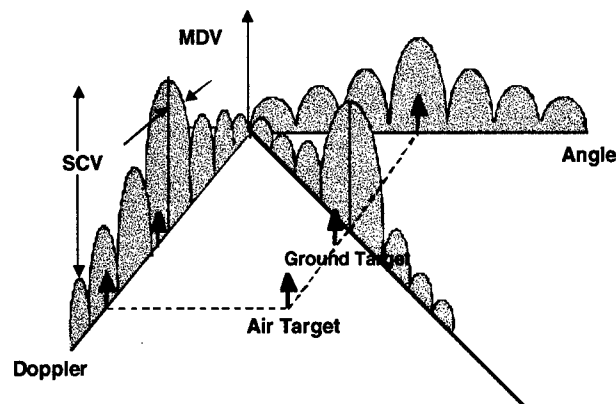


Figure 4 : Angle-Doppler Structure of Clutter

In airborne or space radar, the clutter in a given range cell has a structure determined by the motion of the aircraft platform (Figure 4). The slope of the clutter ridge in angle-Doppler space is determined by the speed of the aircraft. In the AMTI case, the threat target is widely spaced from mainlobe clutter in the Doppler domain and it is possible to use Doppler processing to separate targets from clutter. The limitation on target detection is determined by the sub-clutter visibility (SCV). In the GMTI case, the problem is more difficult since the target is close to the mainbeam clutter in Doppler. Placing a null on mainbeam clutter reduces the gain on target and hence detection performance. The goal of GMTI is to reduce the minimum detectable velocity (MDV), the lowest velocity where a target can be separated from clutter.

Traditionally, the fully adaptive (and optimal) STAP procedure determines the adaptive weights using an estimated covariance matrix, as given by Eqn. (1).

$$\mathbf{w} = \hat{\mathbf{R}}^{-1} \mathbf{s}. \quad (1)$$

In the equation,  $\mathbf{s}$  sets the "look direction", the direction in angle and Doppler being tested for the presence of a target. Note that  $\mathbf{s}$  sets the look direction only, while the actual target may be at a different angle-Doppler point close to the look direction. The covariance matrix,  $\mathbf{R}$ , is estimated by averaging over *secondary data* chosen from range cells close to the range cell of interest (the primary range cell) as given by Eqn. (2) and illustrated in Figure 5.

$$\hat{\mathbf{R}} = \frac{1}{K} \sum_{k=1}^K \mathbf{x}_k \mathbf{x}_k^H. \quad (2)$$

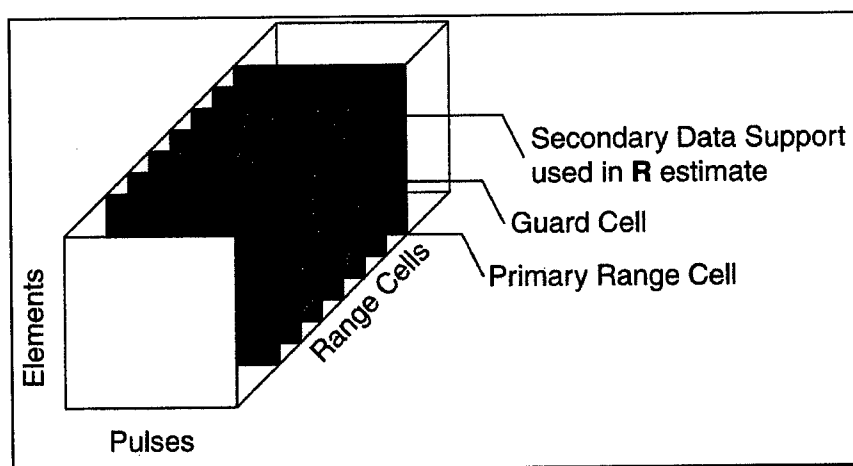
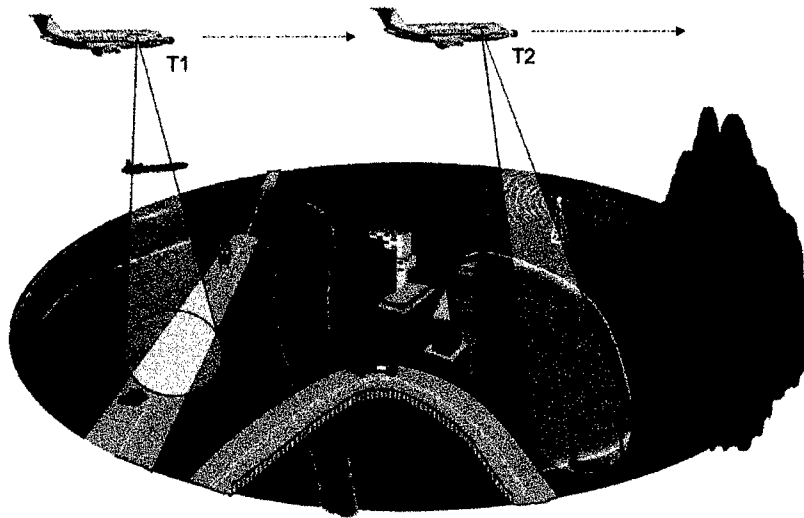


Figure 5 : Estimating the space-time interference covariance matrix

Equations (1) and (2) illustrate the two main difficulties in applying the fully adaptive procedure: the number of degrees of freedom and the assumption of homogeneous data. Underlying several STAP approaches is a third problem, ignoring array effects.

**Computation Load:** In Eqn. (1) the number of unknowns and size of the covariance matrix directly determines the degrees of freedom. The total computation load rises as the third power of the number of unknowns. Choosing this parameter is therefore crucial to a practical implementation of STAP. In the fully adaptive approach, the number of unknowns is the number of antenna subarrays ( $N$ ) times the number of pulses ( $M$ ) in the datacube. The algorithm estimates the  $NM$  dimensional covariance matrix of the interference. In practice, an accurate estimate requires about  $2NM$  to  $3NM$  independent and identically distributed (i.i.d.) secondary data samples [2]. This number is very large making it impossible to evaluate the covariance matrix and the adaptive weights in a reasonable computation time. The goal of STAP research has therefore been to reduce the number of adaptive unknowns, while retaining performance.

### **Homogeneous Data:**



**Figure 6: Clutter Non-Homogeneity**

Equation (2) estimates the covariance matrix using  $K$  secondary data vectors from range bins close to the range cell of interest. The inherent assumption is that the statistics of the interference in the secondary data is the same as that within the primary range cell, i.e. the data is assumed homogeneous.  $K$  must be greater than twice the number of unknowns, between  $2NM$  and  $3NM$  in the fully adaptive case [2]. In practice, it is impossible to obtain a large number of i.i.d. homogeneous secondary data vectors. No clutter scene is perfectly homogeneous and most, if not all, land clutter is sufficiently non-homogeneous to impact performance. In addition, some regions are worse than others: urban clutter, land/sea interfaces (Figure 6). This leads to severely degraded performance.

**Array effects:** Traditionally STAP algorithms were developed for proof-of-concept, assuming the receiving antenna array is a linear array of isotropic point sensors. In practice, such an array is not feasible and the elements must be of some physical size.

This implies that the array not only receives, but also scatters the incident fields, leading to mutual coupling between elements. Additionally, near field scattering off the aircraft body has a significant impact on how the array receives incident signals. Ignoring array effects leads to significantly degraded STAP performance.

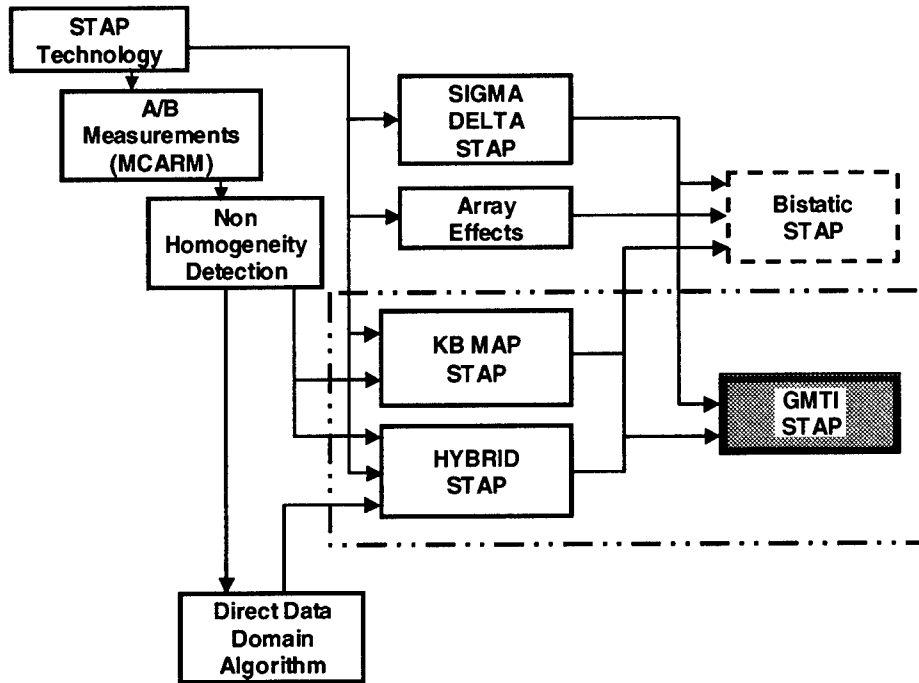


Figure 7: Past and Proposed STAP efforts

AFRL's efforts in STAP have addressed these concerns to enable the transition from theory to practice. Current efforts address the concerns listed in this section while extending STAP to mainbeam clutter rejection and the GMTI problem. In addition, AFRL's expertise is also being extended from monostatic radar to bistatic radar. This report summarizes our approach to addressing these issues for GMTI (Figure 7). The rest of section 2.0 summarizes the approaches developed to mitigate the impact of the above concerns. Section 2.1 presents  $\Sigma\Delta$ -STAP and section 2.2 presents Joint Domain Localized (JDL) Processing as reduced rank (low DOF) alternatives to traditional fully adaptive STAP. Section 2.3 presents JDL processing while accounting for array effects, such as mutual coupling and near field scattering from the aircraft body. Section 2.4 presents a non-homogeneity detector to deal with non-homogeneous received data, while section 2.5 presents an alternative, non-statistical, approach to STAP developed specifically for the non-homogeneous data case.

The various techniques presented in this section represent past AFRL work in the transition from STAP theory to practice. They form a critical component of any future proposed adaptive surveillance system for GMTI.

## 2.1 Sigma-Delta STAP

Historically,  $\Sigma\Delta$ -STAP was proposed to minimize the number of adaptive degrees of freedom, and consequently, the computation load. However a (possibly) more important property of  $\Sigma\Delta$ -STAP is the use of only one sum ( $\Sigma$ ) and one or more difference ( $\Delta$ ) beams. For STAP, a phased array with digitized channels is commonly viewed as necessary. Although significant progress is being made on the phased array front-end electronics, the employment of any STAP scheme with a large number of channels imposes its own set of performance requirements. This is particularly true in terms of channel matching. The high performance required of the electronics in these systems thus makes cost an important issue.  $\Sigma\Delta$ -STAP addresses this issue of affordability, as well as concerns about the clutter non-homogeneity, channel-to-channel calibration, and response pattern effects [3].

$\Sigma\Delta$ -STAP is unique in that it can be retrofitted onto any antenna with analog sum and difference beams. Antenna engineers have excelled in the design of high performance sum and difference beams, whether for phased array or for reflector antennas [4]. This is particularly true in airborne radars where the sum and difference beams are already implemented for monopulse tracking and/or motion compensation.

In this section, we first present the  $\Sigma\Delta$ -STAP principle and algorithms with multiple difference beams. We assume in this work that Wideband Noise Jammers (WNJs) have been suppressed before entering  $\Sigma\Delta$ -STAP, by spatial-only processing (e.g., multiple sidelobe cancelers) incorporated with the sum beam and each difference beam [5]. We identify the advantages and limitations of this STAP approach.

### 2.1.1 $\Sigma\Delta$ -STAP Algorithm Development

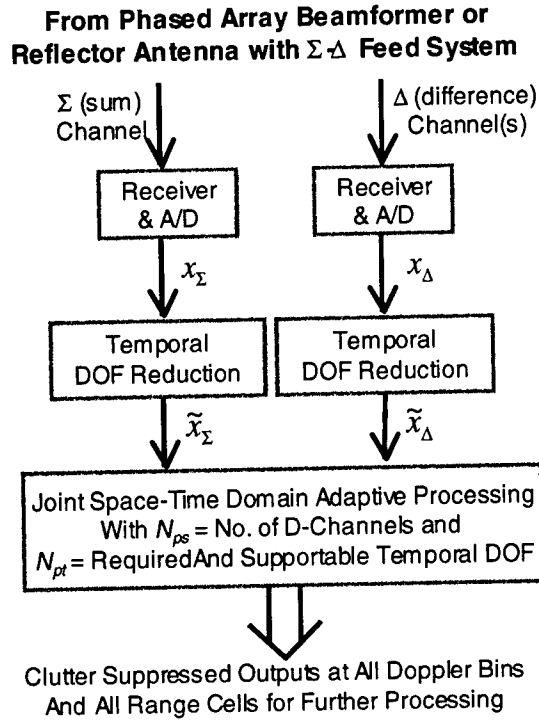


**Figure 8: Block Diagram of General  $\Sigma\Delta$ -STAP**

Figure 8 illustrates the block diagram of general  $\Sigma\Delta$ -STAP where the processor's spatial DOF is determined by  $N_{ps}$ , the number of  $\Delta$ -beams. Much of this block diagram follows the general STAP configuration of [3]. The variations from the block diagram of Figure 8 depend only on the choices of the  $\Delta$ -beams, the temporal DOF reduction approaches, and the joint-domain adaptive filtering-CFAR (constant false alarm rate) algorithms. The algorithm development also makes use of the fact that the  $\Delta$ -beams have deep central nulls in the look direction.

Note that in the block diagram of Figure 8, the sum and difference channels are digitized as opposed to the individual elements themselves.  $\Sigma\Delta$ -STAP treats these channels as equivalent spatial channels and applies adaptive processing to the digitized sum and difference channels. The temporal data from the  $\Sigma$  and  $\Delta$  channels over the  $M$  pulses in a coherent pulse interval (CPI) can be transformed to the Doppler domain, resulting in further DOF reduction.

Let  $x_\Sigma$ , a length  $M$  data vector, be the sum-channel data of a range cell before the temporal DOF reduction. Let  $x_\Delta$ , be the length  $N_{ps}M$  stacked delta-channel data, corresponding to  $N_{ps}$   $\Delta$ -beams, of the same range cell before temporal DOF reduction. If  $N_{pt}$  is the number of unknowns in the temporal domain after DOF reduction, the number of DOF is  $N_{pt}-1$ . The data after reduction can be expressed as



$$\tilde{\mathbf{x}}_{\Sigma} = \mathbf{Q}^H \mathbf{x}_{\Sigma}, \quad (3)$$

and

$$\tilde{\mathbf{x}}_{\Delta} = [\mathbf{I}(N_{ps}) \otimes \mathbf{Q}^H] \mathbf{x}_{\Delta}, \quad (4)$$

where  $\mathbf{Q}$  is a matrix of order  $M \times N_{pt}$  that represents the temporal DOF reduction and  $\otimes$  represents the Kronecker product of two matrices.  $\mathbf{I}(N_{ps})$  is the identity matrix of order  $N_{ps}$ .  $\tilde{\mathbf{x}}_{\Sigma}$  is the post-reduction sum channel data of order  $N_{pt} \times 1$  and  $\tilde{\mathbf{x}}_{\Delta}$  is the post-reduction difference channel data of order  $N_{pt} N_{ps} \times 1$ . The tilde ( $\sim$ ) above the data vectors represents the post-reduction data.

Let  $\mathbf{s}_t$ ,  $M \times 1$ , be the temporal steering vector of a chosen Doppler bin and denote

$$\tilde{\mathbf{s}} = \mathbf{Q}^H \mathbf{s}_t \quad (5)$$

to be the post-reduction temporal steering vector. Denote the stacked data vector

$$\tilde{\mathbf{x}} = \begin{bmatrix} \tilde{\mathbf{x}}_{\Sigma} \\ \tilde{\mathbf{x}}_{\Delta} \end{bmatrix}, \quad (6)$$

Note that  $\tilde{\mathbf{x}}$  simply represents the sum and difference channels after temporal DOF reduction stacked into a convenient form. The “maximum likelihood” estimate of the correlation matrix can be written as

$$\hat{\mathbf{R}} = \begin{bmatrix} \hat{\mathbf{R}}_{\Sigma\Sigma} & \hat{\mathbf{R}}_{\Sigma\Delta} \\ \hat{\mathbf{R}}_{\Delta\Sigma} & \hat{\mathbf{R}}_{\Delta\Delta} \end{bmatrix}, \quad (7)$$

where

$$\hat{\mathbf{R}} = \frac{1}{K} \sum_{k=1}^K \tilde{\mathbf{x}}_k \tilde{\mathbf{x}}_k^H, \quad (8)$$

with  $\tilde{\mathbf{x}}_k$ ,  $k=1, \dots, K$  being secondary data samples from nearby range cells. The adaptive weights are then obtained from Eqn. (1) with the covariance matrix replaced by the estimate given in Eqn. (8). The steering vector is replaced by the post-reduction  $\Sigma\Delta$  steering vector,

$$\tilde{\mathbf{s}} = \begin{bmatrix} \tilde{\mathbf{s}}_t \\ \mathbf{0} \end{bmatrix}, \quad (9)$$

A target at the primary range cell is declared if the modified sample matrix inversion (MSMI) statistic is above a chosen threshold ( $\eta_0$ ).

$$\eta_{MSMI} = \frac{|\hat{\mathbf{w}}^H \tilde{\mathbf{x}}|^2}{\tilde{\mathbf{s}}^H \hat{\mathbf{R}}^{-1} \tilde{\mathbf{s}}} \underset{H_0}{\overset{H_1}{>}} \eta_0. \quad (10)$$

### 2.1.2 Numerical Example

As a numerical example, we compare the performance of  $\Sigma\Delta$ -STAP with the factored approach (FA-STAP) and conventional non-adaptive pulse-Doppler (PD) processing. The array is comprised of 16 elements, with each CPI comprising 16 pulses. This example uses a single  $\Delta$ -channel and temporal DOF reduction reduces the 16 pulses to 3 Doppler bins. As such, there are only 6 unknown weights to be determined: the sum and difference beams in space for 3 Doppler bins. The sum pattern is generated using 35dB Taylor weights and the difference pattern using 30dB Bayliss weights. Possible array errors are modeled as complex Gaussian multiplicative random variables at the element and beamformer level. This example uses a 2% magnitude,  $2^\circ$  phase standard deviation at the element level and a 3% magnitude,  $3^\circ$  phase standard deviation at the beamformer level. The clutter is modeled as Gaussian interference.

Figure 9 compares potential output SINR versus target Doppler for four cases, the fully adaptive case,  $\Sigma\Delta$ -STAP, FA-STAP and traditional, non-adaptive, PD processing [6]. As can be seen, the performance of  $\Sigma\Delta$ -STAP is significantly better than both FA-STAP and PD processing. Of special interest is the performance improvement at low Doppler frequencies, which correspond to low target velocities and consequently the GMTI case.

This example illustrates the significant gains associated with  $\Sigma\Delta$ -STAP. Working with only a limited set of unknowns,  $\Sigma\Delta$ -STAP yields better performance at low Doppler frequencies than algorithms with much higher unknowns (and computation loads). Furthermore, since only the sum and difference beams are used, the algorithm can be applied even if these beams are obtained using analog beamformers.

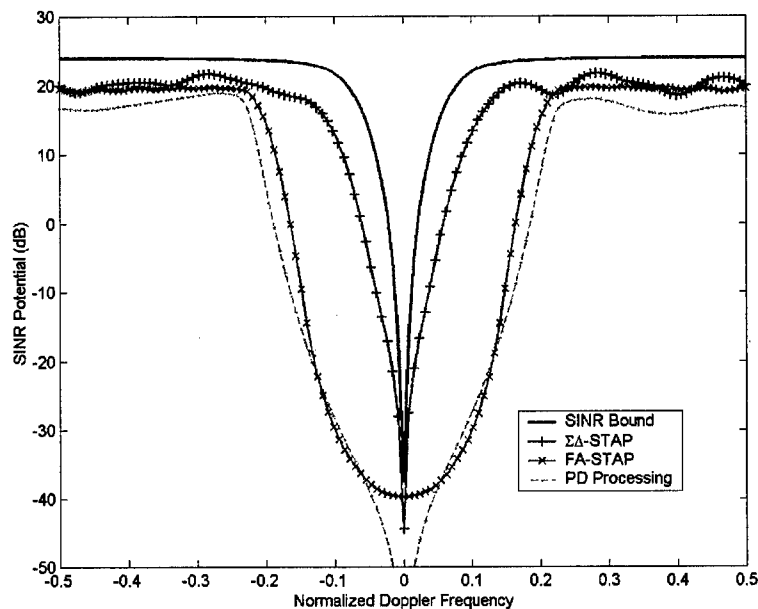


Figure 9: Performance of  $\Sigma\Delta$ -STAP compared to Pulse Doppler processing

### 2.1.3 Discussions: Advantages and Limitations

We summarize the advantages of the  $\Sigma\Delta$ -STAP approach and its limitations. With as few as two spatial channels, Figure 9 shows that the  $\Sigma\Delta$ -STAP approach can lead to clutter suppression performance potential higher than other STAP approaches that require many more unknowns and much higher secondary data support. The following includes its advantages (and some limitations) over other approaches:

**Applicability to Existing Systems:** With other approaches, the application of STAP requires new hardware, from expensive phased arrays to multichannel receivers. In contrast to those approaches, therefore,  $\Sigma\Delta$ -STAP can be applied to existing radar systems, both phased array and continuous aperture. It simply requires digitizing the monopulse difference channel, or making relatively minor antenna modifications to add such a channel. Such a relatively low cost add-on can significantly improve the clutter suppression performance of an *existing* airborne radar system.

**Data Efficiency:** Correlation matrix estimation for  $\Sigma\Delta$ -STAP can be performed with fewer than 20 data vectors. This feature provides good performance in severely non-homogeneous environments where many other STAP approaches may break down, regardless how high their performance potentials are with known clutter statistics.

**Channel Calibration:** Channel calibration is a problem for many other STAP approaches. In order to minimize performance degradation, the channels with many other STAP approaches must be matched across the signal band, and steering vectors must be known to match the array. The difficulty and performance impact of channel

calibration has often been underestimated. In contrast,  $\Sigma\Delta$ -STAP uses as few as two channels to begin with and its corresponding signal (steering) vector remains of known and simple form as long as the central null of the  $\Delta$ -beam is correctly placed. Therefore,  $\Sigma\Delta$ -STAP greatly simplifies calibration issues in practice.

**Response Pattern:** STAP has long been known to have hard-to-predict spatial response patterns that are often undesirable in some applications, e.g., very high sidelobe levels in some interference-free regions, loss of mainlobe gain, and significantly shifted mainlobe peak. With only two spatial channels and with the critical null location of the  $\Delta$ -beam,  $\Sigma\Delta$ -STAP offers much more desirable and predictable response patterns than many other STAP approaches with excessive DOF.

**Computation Load:** While the trend is toward more affordable computing hardware, STAP processing still imposes a considerable burden which increases sharply with the order of the adaptive processor and radar bandwidth. In this respect,  $\Sigma\Delta$ -STAP reduces computational requirements in order  $N^3$  adaptive problems. Moreover, the sparse steering vector can be exploited to further reduce numerical computations.

**Affordability:** Affordability has long been an issue with STAP-based systems. Analog beamforming and minimization of the number of digitized receiver channels provides a substantial payoff in total system cost. Reliability is increased and maintenance costs are reduced by simplifying system interconnects.  $\Sigma\Delta$ -STAP therefore greatly reduces system cost.

**Limitations:** In the case of Doppler ambiguities, any system with only two (or few) channels will not meet the required DOF for clutter suppression.  $\Sigma\Delta$ -STAP is not exceptional in this regard. Additionally, we have established the advantages of the presuppression of WNTs with the needed number of auxiliary channels [5], we do not view that the  $\Sigma\Delta$ -STAP is limited to jammer-free applications. However, there is a need for additional hardware for operation in the presence of jammers.

In summary,  $\Sigma\Delta$ -STAP is a very natural combination of the traditional antenna-design based approaches and "modern" signal processing based approaches, making the best use of the strengths of each and avoiding their weaknesses. The advantages of  $\Sigma\Delta$ -STAP, especially applicability to existing radar systems, far outweigh the limitations of this adaptive processing method.

The next section presents another low computation load algorithm: Joint Domain Localized Processing.

## 2.2 Joint Domain Localized Processing in the Ideal Case

To overcome the drawbacks of the fully adaptive algorithm, researchers have limited the number of adaptive weights to reduce problems associated with sample support and computation expense. Wang and Cai [7] introduced the JDL algorithm, a post-Doppler, beamspace approach that adaptively processes the radar data after transformation to the angle-Doppler domain. Adaptive processing is restricted to a localized processing region (LPR) in the transform domain, significantly reducing the number of unknowns while retaining maximal gain against thermal noise. The reduced DOF leads to corresponding reductions in required sample support and computation load.

This section develops the JDL algorithm as applied to the case of an ideal array. Based on the assumption of a linear array of equispaced, isotropic, point sensors, the space-time data is transformed to the angle-Doppler domain using a two dimensional Fast Fourier Transform (FFT). Under certain restrictions, this approach is valid because the spatial and temporal steering vectors form Fourier coefficients [8, pp. 12-17]. In order to highlight the restrictions placed on the algorithm by the original formulation, this section clarifies the original development of Wang and Cai [7]. Section 2.3 extends the JDL algorithm to account for array effects and illustrates the performance of the JDL algorithm.

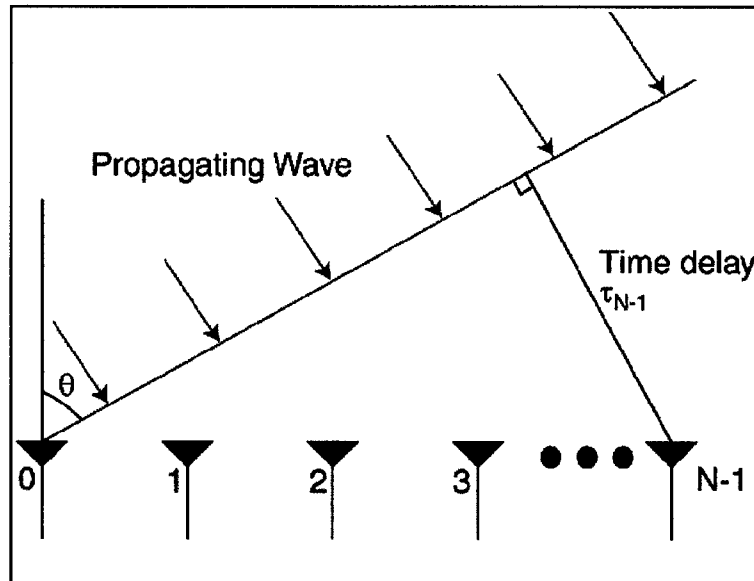


Figure 10: Linear Array of Point Sensors

Consider an equispaced linear array of  $N$  isotropic, point sensors as shown in Figure 10. Each sensor receives data samples corresponding to the  $M$  pulses in a CPI. Therefore, for each range bin, the received data is a length  $MN$  vector  $\mathbf{x}$  whose entries numbered  $mN$  to  $[(m + 1)N - 1]$  correspond to the returns at the  $N$  elements from pulse number  $m$ , where  $m = 0, 1, \dots, M - 1$ . The data vector is a sum of the contributions from the external interference sources, the thermal noise and possibly a target, i.e.

$$\mathbf{x} = \xi \mathbf{s}(\phi_t, f_t) + \mathbf{c} + \mathbf{n} \quad (11)$$

where  $\mathbf{c}$  is the vector of interference sources,  $\mathbf{n}$  is the thermal noise and  $\xi$  is the target amplitude, equal to zero in range cells without a target. The term  $\mathbf{s}(\phi_t, f_t)$  is the space-time steering vector corresponding to a possible target at look angle  $\phi_t$  and Doppler frequency  $f_t$ . The steering vector can be written in terms of a spatial steering vector  $\mathbf{a}(\phi_t)$  and a temporal steering vector  $\mathbf{b}(f_t)$  [8],

$$\mathbf{s}(\phi_t, f_t) = \mathbf{b}(f_t) \otimes \mathbf{a}(\phi_t), \quad (12)$$

$$\mathbf{a}(\phi_t) = [1 \ e^{j2\pi f_s} \ e^{j(2)2\pi f_s} \ \dots \ e^{j(N-1)2\pi f_s}]^T, \quad (13)$$

$$\mathbf{b}(f_t) = [1 \ e^{j2\pi f_t / f_R} \ e^{j(2)2\pi f_t / f_R} \ \dots \ e^{j(M-1)2\pi f_t / f_R}]^T, \quad (14)$$

where  $f_s$  is the normalized spatial frequency given by  $f_s = (d/\lambda)\sin\phi_t$ ,  $\lambda$  the wavelength of operation and  $f_R$  the pulse repetition frequency (PRF).

The spatial steering vector  $\mathbf{a}(\phi)$  is the magnitude and phase taper at the  $N$  elements of the array due to a far field source at angle  $\phi$ . Owing to electromagnetic reciprocity, to transmit in the direction of  $\phi$  the elements of the array must be excited with the conjugates of the steering vector, i.e. the conjugates of the steering vector maximize the response in the direction  $\phi$ . Transformation of spatial data to the angle domain at angle  $\phi$  therefore requires an inner product with the corresponding spatial steering vector. Similarly, the temporal steering vector  $\mathbf{b}(f)$  corresponding to a Doppler frequency  $f$  is the magnitude and phase taper measured at an individual element for the  $M$  pulses in a CPI. An inner product with the corresponding temporal steering vector transforms time domain data to the Doppler domain. The angle-Doppler response of the data vector  $\mathbf{x}$  at angle  $\phi$  and Doppler  $f$  is therefore given by

$$\tilde{\mathbf{x}}(\phi, f) = [\mathbf{b}(f) \otimes \mathbf{a}(\phi)]^H \mathbf{x}, \quad (15)$$

where the tilde ( $\sim$ ) above the scalar  $\mathbf{x}(\phi, f)$  signifies the post-transform angle-Doppler domain. Choosing a set of spatial and temporal steering vectors generates a corresponding vector of angle-Doppler domain data.

Equations (12)-(14) show that for an ideal array the spatial and temporal steering vectors are identical to the Fourier coefficients. Based on this observation, the transformation to the angle-Doppler domain can be simplified under two conditions.

- If a set of angles are chosen such that  $(d/\lambda \sin \phi)$  is spaced by  $1/N$  and a set of Doppler frequencies are chosen such that  $(f/f_R)$  is spaced by  $1/M$ , the transformation to the angle-Doppler domain is equivalent to the 2D.DFT.
- If the angle  $\phi_k$  corresponds to one of these angles *and* the Doppler  $f$  corresponds to one of these Dopplers, the steering vector is a column of the 2-D DFT matrix and the angle-Doppler steering vector is localized to a single angle-Doppler bin (Figure 11).

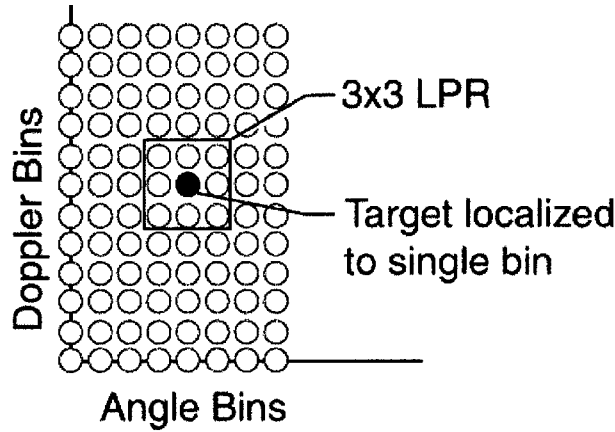


Figure 11: Localized Processing Regions in JDL for  $\eta_a = \eta_d = 3$

The JDL algorithm as originally developed in [7] assumes both these conditions are met. This simplification is possible only in the case of the ideal, equispaced, linear array of Figure 10. Owing to beam mismatch, the localization to a single point in angle-Doppler space is only exact for the look steering vector.

As shown in Figure 11, a LPR centered about the look angle-Doppler point is formed and interference is suppressed in this angle-Doppler region only. The LPR covers  $\eta_a$  angle bins and  $\eta_d$  Doppler bins. The choice of  $\eta_a$  and  $\eta_d$  is independent of  $N$  and  $M$ , i.e. the localization of the target to a single angle-Doppler bin decouples the number of adaptive degrees of freedom from the size of the data cube, while retaining maximal gain against thermal noise. The covariance matrix corresponding to this LPR is estimated using secondary data from neighboring range cells. The adaptive weights are then calculated using Eqn. (1). The estimated covariance matrix  $\hat{\mathbf{R}}$  is replaced with  $\tilde{\mathbf{R}}$ , the estimated *angle-Doppler* covariance matrix corresponding to the LPR of interest. The steering vector  $\mathbf{s}$  is replaced with the angle-Doppler steering vector  $\tilde{\mathbf{s}}$ , i.e.

$$\tilde{\mathbf{w}} = \tilde{\mathbf{R}}^{-1} \tilde{\mathbf{s}}. \quad (16)$$

The number of adaptive unknowns is equal to  $\eta_a \eta_d$ . The steering vector for the adaptive process is the space-time steering vector  $\mathbf{s}$  of Eqn. (12) transformed to the

angle-Doppler domain. Under the two conditions listed above  $\tilde{\mathbf{s}}$  is given by the length  $\eta_a \eta_d$  vector

$$\tilde{\mathbf{s}} = [0, 0, \dots, 0, 1, 0, \dots, 0, 0]^T. \quad (17)$$

It must be emphasized that this simple form of the steering vector is valid only because the DFT is an orthogonal transformation. The space-time steering vector is transformed to angle-Doppler using the same transformation used for the data.

### 2.3 JDL Processing Accounting for Array Effects

Sections 2.1 and 2.2 presented two adaptive processing algorithms that address the issue of minimizing the number of adaptive unknowns while maintaining system performance. Reducing the number of unknowns leads to corresponding reductions in required sample support (to estimate the covariance matrix) and computation load (to obtain the adaptive weights). This section addresses a second major concern: the impact of mutual coupling between the elements of the array and the scattering off the aircraft body. The results in this section were published in [9].

When applying the JDL algorithm to measured data, a crucial assumption in the development of [7] is invalid. The elements of a real array cannot be point sensors. Owing to their physical size, the elements of the array are subject to mutual coupling. Furthermore, the assumption of a linear array is restrictive. A planar array allows for DOF in azimuth and elevation. Therefore the Fourier coefficients do not form the spatial steering vector and a DFT does not transform the spatial data to the angle domain. In this case, a DFT is mathematically feasible but has no physical meaning.

In a physical array, the spatial steering vectors must be measured or obtained using a numerical electromagnetic analysis. These steering vectors must be used to transform the space domain to the angle domain. This transformation is necessarily non-orthogonal with a corresponding spread of target information in the angle-Doppler domain. The assumptions listed in Section 2.2, therefore, cannot be met in practice. Earlier attempts to apply JDL to a real array ignored the non-orthogonal nature of the measured spatial transform [10].

This section replaces the DFT-based transformation described in Section 2.2 with a generalized transformation matrix. The key contribution of this new approach is the accounting for the array effects, thereby eliminating the two stipulations on the original JDL algorithm. This formulation can now be applied to physical arrays of arbitrary configuration. The modification results in significantly improved detection performance.

In the JDL algorithm, only data from within the LPR is used for the adaptation process. The transformation from the space-time domain to the angle-Doppler domain is an inner product with a space-time steering vector, an argument that holds true for ideal



linear arrays and physical arrays. Mathematically therefore, the relevant transformation to within the LPR is a pre-multiplication with a  $(NM \times \eta_a \eta_d)$  transformation matrix. The transformation process is

$$\tilde{\mathbf{x}}_{LPR} = \mathbf{T}^H \mathbf{x}. \quad (18)$$

For example, for an LPR of 3 angle bins  $(\phi_{-1}, \phi_0, \phi_1; \eta_a=3)$  and 3 Doppler bins  $(f_{-1}, f_0, f_1; \eta_d=3)$

$$\begin{aligned} \mathbf{T} &= [\mathbf{b}(f_{-1}) \otimes \mathbf{a}(\phi_{-1}) \quad \mathbf{b}(f_{-1}) \otimes \mathbf{a}(\phi_0) \quad \mathbf{b}(f_{-1}) \otimes \mathbf{a}(\phi_1) \\ &\quad \mathbf{b}(f_0) \otimes \mathbf{a}(\phi_{-1}) \quad \mathbf{b}(f_0) \otimes \mathbf{a}(\phi_0) \quad \mathbf{b}(f_0) \otimes \mathbf{a}(\phi_1) \\ &\quad \mathbf{b}(f_1) \otimes \mathbf{a}(\phi_{-1}) \quad \mathbf{b}(f_1) \otimes \mathbf{a}(\phi_0) \quad \mathbf{b}(f_1) \otimes \mathbf{a}(\phi_1)], \\ &= [\mathbf{b}(f_{-1}) \quad \mathbf{b}(f_0) \quad \mathbf{b}(f_1)] \otimes [\mathbf{a}(\phi_{-1}) \quad \mathbf{a}(\phi_0) \quad \mathbf{a}(\phi_1)]. \end{aligned} \quad (19)$$

In [7], to achieve the simple form of the angle-Doppler steering vector given by Eqn. (17), the use of a low sidelobe window to lower the transform sidelobes is discouraged. However, the use of such a window may be incorporated by modifying the transformation matrix of Eqn. (19). If a length  $N$  taper  $\mathbf{t}_s$  is to be used in the spatial domain and a length of  $M$  taper  $\mathbf{t}_t$  in the temporal domain, the transformation matrix is given by

$$\mathbf{T} = [\mathbf{t}_t \bullet \mathbf{b}(f_{-1}) \quad \mathbf{t}_t \bullet \mathbf{b}(f_0) \quad \mathbf{t}_t \bullet \mathbf{b}(f_1)] \otimes [\mathbf{t}_s \bullet \mathbf{a}(\phi_{-1}) \quad \mathbf{t}_s \bullet \mathbf{a}(\phi_0) \quad \mathbf{t}_s \bullet \mathbf{a}(\phi_1)] \quad (20)$$

where  $\bullet$  represents the Hadamard product, a point-by-point multiplication of two vectors.

The angle-Doppler steering vector used to solve for the adaptive weights in Eqn. (16) is the space-time steering vector, transformed to the angle-Doppler domain via the same transformation matrix  $\mathbf{T}$ , i.e.

$$\tilde{\mathbf{s}} = \mathbf{T}^H \mathbf{s} \quad (21)$$

Note the transformation matrix defined in Eqn. (20) is defined for the chosen Doppler frequencies and angles without any restrictions on their values. No assumption is made about the form of the spatial or temporal steering vectors, i.e. the use of a transformation matrix eliminates the two restrictions of the original JDL formulation.

In the case of a linear array of isotropic point sensors, the ideal steering vectors are obtained from Eqns. (13) and (14). If the angles and Doppler frequencies satisfy the conditions listed in Section 2.2, the transformation matrix  $\mathbf{T}$  reduces to the relevant rows of the 2-D FFT matrix. The FFT-based formulation is equivalent to choosing a spacing in

the angle domain such that  $[(d/\lambda)\Delta\sin(\phi)]=1/N$  and in the Doppler domain of  $\Delta f=1/M$ . Furthermore, if both the look angle and Doppler correspond to one of these angles and Dopplers, the transformed steering vector of Eqn. (21) is equivalent to the steering vector of Eqn. (17). The formulation of [7] is therefore a special, not necessarily optimal, case of the more general formulation presented here.

For a real array, the steering vector associated with a given angle is the measured magnitude and phase taper due to a calibrated far-field source. If measurements are not available, the steering vectors can be obtained from a numerical electromagnetic analysis of the receiving antenna. These steering vectors include array effects and the effects that the aircraft body has on the reception of signals. Usually, even in the case of a real array, the pulses are equally spaced in time and hence the temporal steering vector is unchanged. In the case of a real array, the spatial component in Eqn. (12) must be replaced with a measured steering vector, i.e. the space time steering vector is:

$$\mathbf{s}(\phi_t, f_t) = \mathbf{b}(f_t) \otimes \mathbf{a}_m(\phi_t), \quad (22)$$

where  $\mathbf{a}_m(\phi_t)$  is the *measured* steering vector corresponding to angle  $\phi_t$ . Similarly the spatial steering vectors in the transformation matrix of Eqns. (19) and (20) must be replaced with the corresponding measured steering vectors.

Melvin and Himed [10] applied the JDL algorithm to measured data and used the measured steering vectors to transform the space domain to the angle domain. In effect, without explicitly stating so, they use a transformation matrix in the spatial domain and a DFT in the temporal domain. The spacing between the angles chosen for the LPR is determined by the available measured steering vectors. The spacing between the Doppler frequencies is fixed by the DFT. Crucially, the resulting change on the angle-Doppler steering vector is ignored and they assume the simplified form of the steering vector in Eqn. (17) is valid. However, the use of a different transform from the spatial domain to the angle domain violates the assumptions listed in Section 2.2.

### 2.3.1 Multi-Channel Airborne Radar Measurements (MCARM)

The discussion above dealt with applying the JDL algorithm to real arrays by accounting for array and airframe effect. The performance improvements over the original JDL algorithm are presented here using data from the MCARM database.

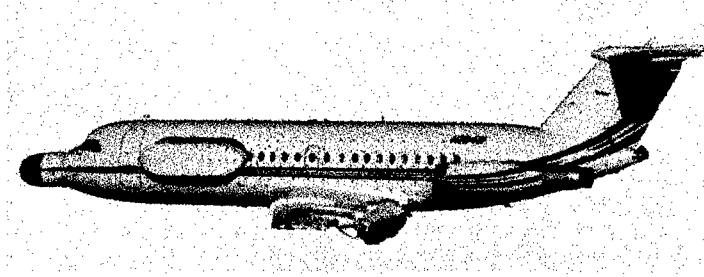


**Figure 12: MCARM Testbed**

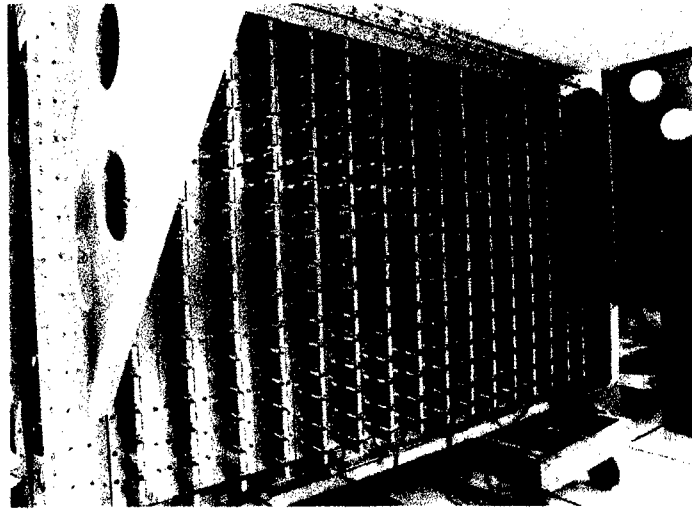


**Figure 13: MCARM Antenna Array**

The MCARM program had as its objective the collection of multiple spatial channel airborne radar data for the development and evaluation of STAP algorithms for future Airborne Early Warning (AEW) radar systems. The Air Force Research Laboratory contracted with Northrop Grumman to develop the measurement capability and to accomplish the flight tests [11, 12].

Under the MCARM program, some Northrop Grumman ground moving target indication (GMTI) data was collected with and without vegetation to evaluate foliage penetration (FOPEN). Mono-static data was collected at PRFs of 7 kHz, 2 kHz, and 500 Hz. The MCARM data was collected by Northrop Grumman during flights over the Delmarva Peninsula and the east coast of the US. There were a total of eleven flights with more than 50 Gigabytes of data collected.

To leverage current computer and software technology AFRL has implemented a web site at <http://128.132.42.229/>. A researcher can access the site, fill out, and submit an application to obtain access to the processed radar data. Also available are copies of the Northrop Grumman final report and relevant research papers. Once the researcher's application is approved, data can be retrieved from the web site for internal use. The data

we are using for this effort has been obtained from this site. We chose this data because of its varied and heterogeneous clutter environment.

The airborne MCARM testbed, a BAC1-11 aircraft, used for these measurements is shown in Figure 12. The sensor is hosted in an aerodynamic cheek-mounted, mounted just forward of the left wing of the aircraft. The L-band (1.24GHz) active array consists of 16 columns, with each column having two 4-element subarrays (Figure 13). The elements are vertically polarized, dual-notch reduced-depth radiators. These elements are located on a rectangular grid with azimuth spacing of 4.3 inches and elevation spacing of 5.54 inches. There is a 20 dB Taylor weighting across the 8 elevation elements resulting in a 0.25 dB elevation taper loss for both transmit and receive. The total average radiated power for the array was approximately 1.5 kW. A 6 dB modified trapezoid weighting for the transmit azimuthal illumination function is used to produce a  $7.5^\circ$  beamwidth pattern on boresight with -25 dB rms sidelobes. This pattern can be steered up to  $\pm 60^\circ$ .

Of the 32 possible channels, only 24 receivers were available for the data collection program. Two of the receivers were used for analog sum and azimuthal difference beams. There are therefore 22 ( $N=22$ ) digitized channels which, in this work, are arranged as rectangular  $2 \times 11$  array. Each CPI comprises 128 ( $M=128$ ) pulses at a PRF of 1984Hz.

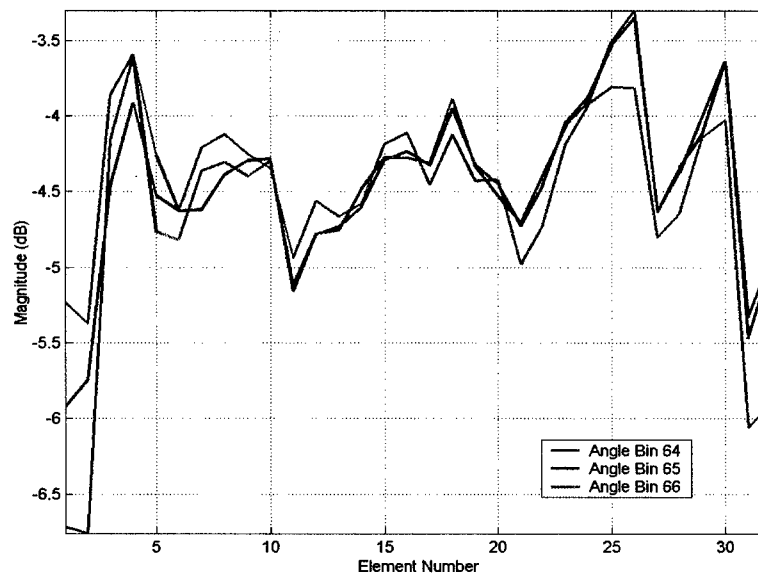


**Figure 14: Magnitude of MCARM steering vectors**

In the ideal case of a linear array, Eqn. (13) shows that the magnitude of the steering vector is constant at each element. Figure 14 shows the variation in magnitude for the MCARM array. The magnitude varies by as much as 4dB over the 32 elements. This variation is due to the mutual coupling between the elements of the antenna array.

### 2.3.2 Example 1. Injected target

In the first example, a synthetic target of fixed amplitude, direction, Doppler and range is injected into the MCARM data set. The amplitude and phase variation of the injected target across the 22 channels is obtained from the measured steering vectors. The amplitude of the injected target is chosen such that it remains undetected by non-adaptive pulse-Doppler processing.

JDL processing is performed at the target angle bin, for a few range bins surrounding the injected target and for all Doppler bins. In this example, the figure of merit used to compare the two scenarios is the separation between the MSMI statistic at the target range/Doppler bin and the highest statistic at other range or Doppler bins (the largest false alarm statistic). A large separation implies a large difference between target and residual interference, i.e. improving the ability to detect the target.

In this example, the data from acquisition 575 on flight 5 is used. The parameters of the injected target are: Amplitude =  $0.0001 \angle 0^\circ$ , Angle bin =  $0^\circ$  (Broadside), Doppler bin = -9 (-139.5Hz), Range bin = 290

Figure 15 plots the MSMI statistic, as a function of range bin for the two scenarios considered. In the first case, a strong false alarm several dB over the target is clearly visible. In the second case, target clearly stands out over the nearest false alarm. The false alarm is somewhat suppressed, but more crucially, the gain on the target and hence the target statistic is significantly improved. Accounting for the non-orthogonal nature of the steering vectors yields an improvement of 7.1dB.

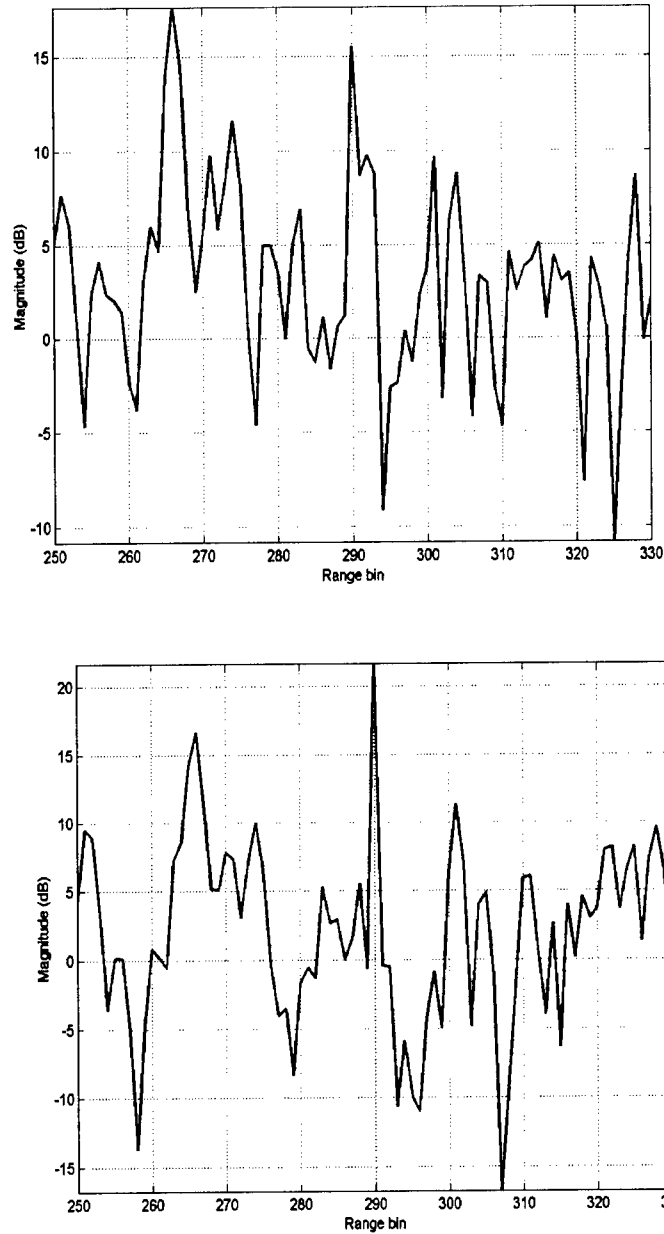


**Figure 15: JDL performance before and after accounting for array effects (Injected Target)**

### 2.3.3 Example 2: MTS Tones

On flight 5, acquisition 152 includes clutter and tones from a moving target simulator (MTS) at pre-selected Doppler frequencies. Five tones are received at approximately -800 Hz (0 dB), -600 Hz (-14 dB), -400 Hz (-20 dB), -200 Hz (-26 dB) and 0 Hz (-31 dB). The data in this acquisition are returns from 128 pulses measured across 22 channels. The pulse repetition frequency for this flight was 1984 Hz, hence the separation of 200 Hz corresponds to nearly 13 Doppler bins. Using an acquisition with the MTS allows us to compare the performance of the JDL algorithm in the above scenarios using measured data. The MTS tones are processed like returns from moving targets. The presence of

five MTS tones of differing amplitudes makes it difficult to define a unique figure of merit to compare the two scenarios. In this example, a visual inspection is used for comparison.

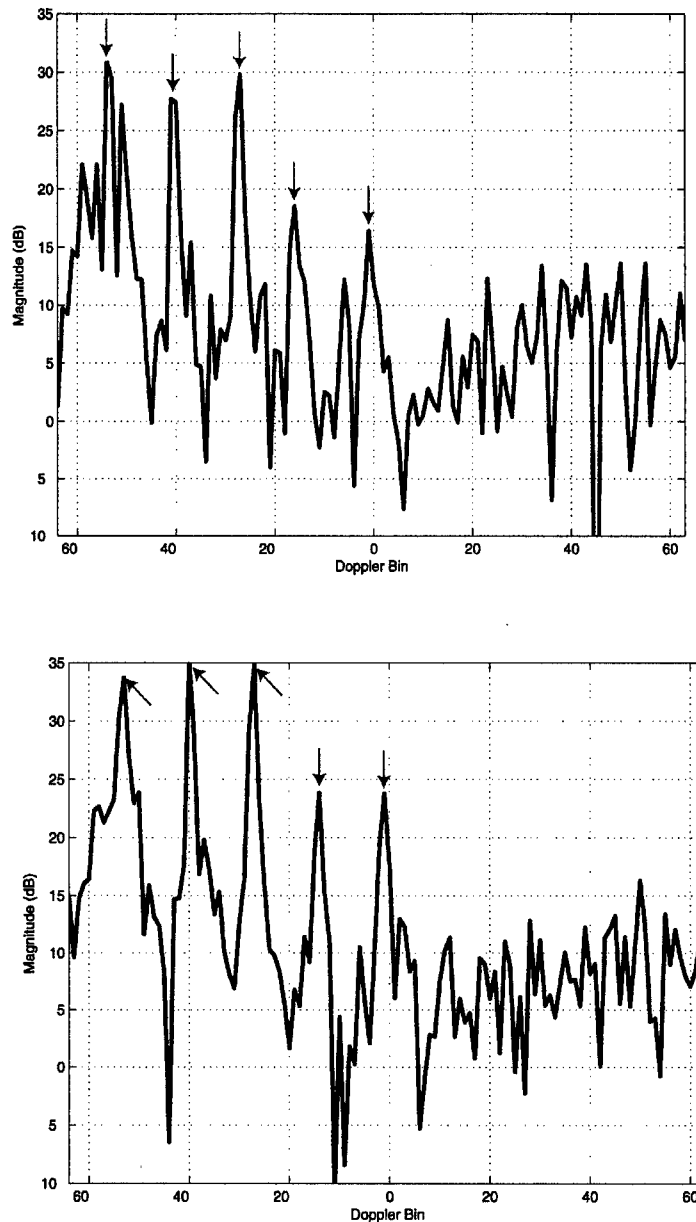


**Figure 16: JDL before and after accounting for array effects (MTS Tones)**

Figure 16 plots the MSML statistic versus Doppler bin for the two cases considered. In the first plot, the five tones are clearly visible with the strongest tone at bin -53 spread over Doppler space. A few spurious tones are also visible. The second plot shows the results of the JDL algorithm modified by Eqn. (21). The five tones are clearly visible and the spurious tones are completely suppressed.

Figure 15 and Figure 16 demonstrate the importance of and performance enhancements possible by accounting for array effects. The traditional formulation for JDL ignored the fact that real world arrays are not comprised of isotropic, point sensors. Accounting for the array effects leads to huge improvements in performance, *as applied to measured data*.

## 2.4 Non-Homogeneity Detection/Knowledge Based Processing

This section presents the third of the key issues that limit the performance of adaptive processing algorithms in real world applications: the non-homogeneous and dynamic background environments typically observed from airborne radar. Non-homogeneous data is the most significant of the three issues that we discuss. Significant processing losses result from mismatches between the environment and the processing algorithms. Recent work has shown that it is essential to sense the actual environment, and then to match end-to-end processing to this environment. Moreover, the processing should be "intelligent"; the radar processor should learn from the environment.

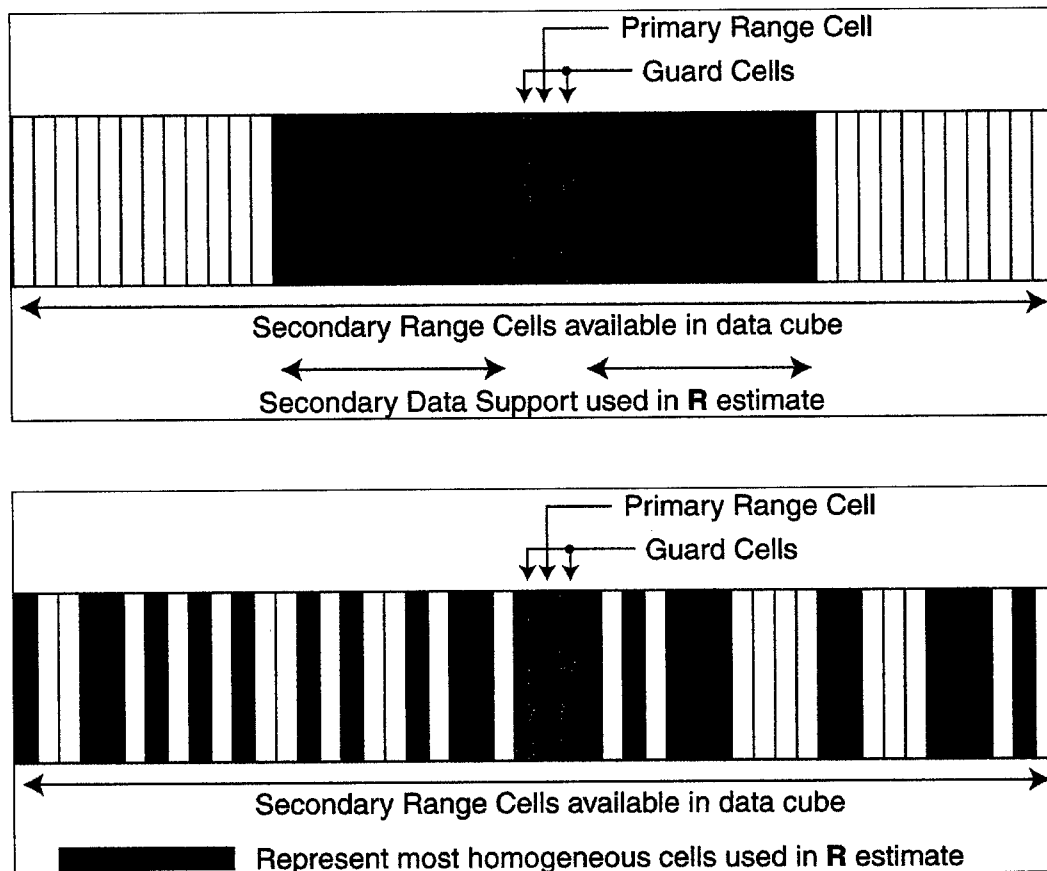


Figure 17: Secondary Data Selection (a) Homogeneous Case (b) Non-homogeneous Case

In the filtering and detection stages of the radar processing chain, training data are selected about the cell under test, and that training data is used to represent the interference in the cell under test. Conventional constant false alarm rate (CFAR) and



space-time adaptive processing (STAP) algorithms use a symmetric sliding window about the cell under test in order to select the training data as shown in Figure 17(a). This assumes that the data is homogeneous and i.i.d. To quote [13] "A data set is termed wide sense homogeneous if the system performance loss can be ignored or is acceptable for a given STAP algorithm. A data set is said to be wide sense non-homogeneous if it is not wide sense homogeneous". In the real world, wide sense homogeneity is routinely violated, leading to sub-optimum performance.

Improved methods are needed to more carefully select processing based on the environment. For detection and filtering, this means better selection of training data, requiring non-symmetric secondary data samples be selected. As shown in Figure 17(b) these secondary data samples must best represent the interference, or at least the homogeneous component of the interference, in a statistical sense.

The non-homogeneity detector (NHD) must be matched to the processing at hand. For example, a non-homogeneity that impacts on the performance of FA-STAP has no impact on the performance of the JDL algorithm if it falls in a natural null of the transformation to the angle-Doppler domain. Transforms to other domains may therefore be necessary. Figure 18 shows non-homogeneity detection in two different domains. In the upper path, range-pulse-element data cubes are transformed into angle-Doppler space for non-homogeneity detection in a two-dimensional LPR. This form of NHD is well suited for the JDL algorithm. In the lower path, a one-dimensional transform is executed and non-homogeneity detection is performed in element-Doppler space. The nature of the data may also dictate whether full- or reduced-dimension adaptive algorithms be executed. If the sample support is severely limited, direct data domain, non-statistical, adaptive algorithms may be required.

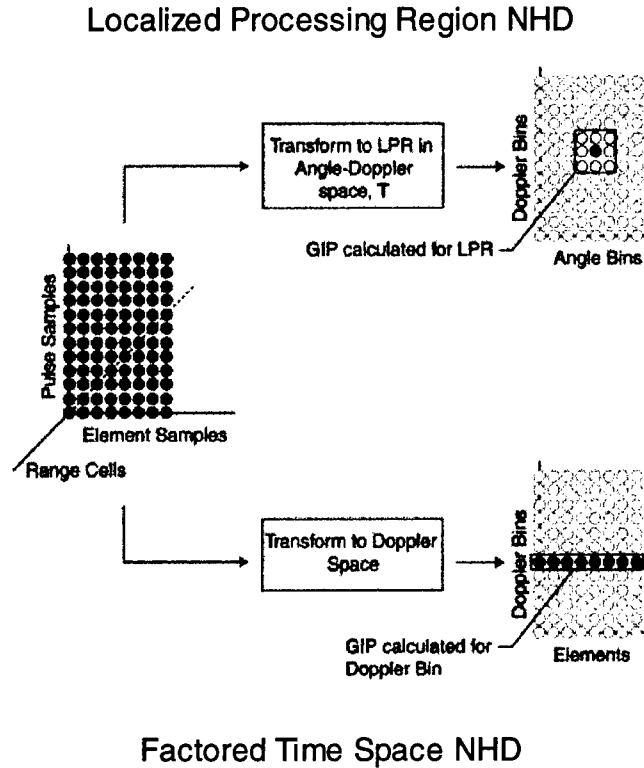


**Figure 18: Non-Homogeneity Detection in LPR and in Factored Approaches**

Recent developments in non-homogeneity detection allow for better selection of training data. AFRL has been investigating a variety of non-homogeneity detection techniques including application of the Generalized Inner Product and multi-pass STAP. In multi-pass STAP techniques, a first filtering stage serves as the non-homogeneity detector (NHD). A second stage then performs the filtering function. This formulation will be explained in detail later in this report.

Using a NHD provides significant performance improvement over conventional methods. However, once non-homogeneous cells have been identified, how are these cells handled in the filtering and detection processes? By definition, the non-homogeneous cells are not like neighboring cells, so it is not appropriate to use traditional statistical techniques, which estimate the interference in the cell under test by covariance matrix estimation. To address these cases, AFRL is continuing to develop hybrid STAP techniques that combine direct data domain (non-statistical) and sample covariance matrix based (statistical) adaptive processing.

## **2.5 Direct Least Squares Approach**

The inability of traditional statistical algorithms to counter the non-homogeneous component of interference motivates research in non-statistical or direct data domain ( $D^3$ ) algorithms.

In [14] an algorithm is developed that optimizes the signal to interference in a least squares sense for signals at the angle at which a look-direction constraint is established. This method minimizes, in a least squares sense, the error between the received voltages (signal plus interference) and a signal from the assumed angle. This approach does not employ data from outside the radar range cell being evaluated, i.e. this approach does not require secondary data. This makes the  $D^3$  an attractive alternative in non-homogeneous clutter. This is especially true in a severely non-homogeneous clutter environment of urban and land/sea interfaces. The  $D^3$  approach has recently focused on one-dimensional spatial adaptivity [14]. This section introduces a new two-dimensional space-time  $D^3$  algorithm based on the one-dimensional algorithm of [14].

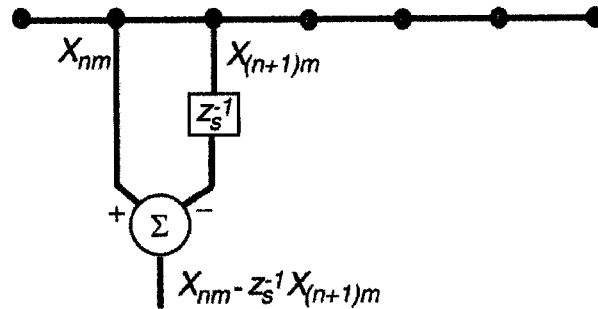


Figure 19: Principle of Direct Data Domain Processing

Consider the  $N$ -element uniformly spaced array shown in Figure 19. For a look direction of  $\phi_s$ , the signal advances from one element to the next by the same phase factor  $z_s = [\exp(j2\pi \sin(\phi))]$ . The term obtained by the subtraction operation in Figure 19 is *therefore free of the target signal and contains only interference terms*. The  $D^3$  algorithm minimizes the power in such interference terms while maintaining gain in the direction of the target.

To best present the  $D^3$  algorithm, the data from the  $N$  elements due to the  $M$  pulses in a CPI is written as a  $N \times M$  matrix  $\mathbf{X}$  whose  $m^{\text{th}}$  column corresponds to the  $N$  returns from the  $m^{\text{th}}$  pulse, represented by  $\mathbf{x}(m)$ . The data matrix is a sum of target and interference terms. Rewriting Eqn. (11) in terms of matrices

$$\mathbf{X} = \xi \mathbf{S}(\phi_t, f_t) + \mathbf{C} + \mathbf{N}. \quad (23)$$

Define the  $M \times (N-1)$  matrix  $\mathbf{A}$  to be

$$\mathbf{A} = \begin{bmatrix} \mathbf{X}_{00} - z_s^{-1} \mathbf{X}_{10} & \mathbf{X}_{10} - z_s^{-1} \mathbf{X}_{20} & \cdots & \mathbf{X}_{(N-2)0} - z_s^{-1} \mathbf{X}_{(N-1)0} \\ \mathbf{X}_{01} - z_s^{-1} \mathbf{X}_{11} & \mathbf{X}_{11} - z_s^{-1} \mathbf{X}_{21} & \cdots & \mathbf{X}_{(N-2)1} - z_s^{-1} \mathbf{X}_{(N-1)1} \\ \vdots & \vdots & \vdots & \vdots \\ \mathbf{X}_{0(M-1)} - z_s^{-1} \mathbf{X}_{1(M-1)} & \mathbf{X}_{1(M-1)} - z_s^{-1} \mathbf{X}_{2(M-1)} & \cdots & \mathbf{X}_{(N-2)(M-1)} - z_s^{-1} \mathbf{X}_{(N-1)(M-1)} \end{bmatrix}, \quad (24)$$

where  $z_s$ , as defined earlier, is the phase progression of the *target signal* from one element to the next. Theoretically, the entries of  $\mathbf{A}$  are interference terms only, though due to beam mismatch there may be some residual signal power. However, unless the target is significantly off the look direction/Doppler, the target signal is effectively nulled. In case the target is significantly off the look direction, it must be treated as interference: in a surveillance radar, targets must be declared only if they are in the look direction. In fact, sidelobe targets are an example of the discrete, non-homogeneous, interference that drives this research.

Consider the following scalar functions of a vector of spatial weights  $\mathbf{w}_s$ .

$$\begin{aligned} G_{\mathbf{w}_s} &= \left| \mathbf{w}_s^H \mathbf{a}_{(0:N-2)} \right|^2 = \mathbf{w}_s^H \mathbf{a}_{(0:N-2)} \mathbf{a}_{(0:N-2)}^H \mathbf{w}_s, \\ I_{\mathbf{w}_s} &= \left\| \mathbf{A}^* \mathbf{w}_s \right\|^2 = \mathbf{w}_s^H \mathbf{A}^T \mathbf{A}^* \mathbf{w}_s, \\ R_{\mathbf{w}_s} &= G_{\mathbf{w}_s} - \kappa^2 I_{\mathbf{w}_s}, \end{aligned} \quad (25)$$

where  $\|\cdot\|$  represents the 2-norm of a vector and  $\mathbf{a}_{(0:N-2)}$  represents the first  $N-1$  entries of the spatial steering vector. In the equation,  $\mathbf{A}^* \mathbf{w}_s$  is used to remain consistent with the term  $\mathbf{w}_s^H \mathbf{a}_{(0:N-2)}$  in that the weights multiply the conjugate of the data.

The term  $G$  in Eqn. (25) represents the gain of the weight vector  $\mathbf{w}_s$  at the look angle  $\phi$ , while the term  $I$  represents the residual interference power after the data is filtered by the same weights. Hence, the term  $R$  is the difference between the gain of the antenna at the look Doppler and the residual interference power. The term  $\kappa$  in the definition of  $R$  is an emphasis parameter that will be described later. The  $D^3$  algorithm finds the weights that maximize this difference. Mathematically,

$$\begin{aligned} \max_{\|\mathbf{w}_t\|_2=1} [R_{\mathbf{w}_t}] &= \max_{\|\mathbf{w}_t\|_2=1} [G_{\mathbf{w}_t} - \kappa^2 I_{\mathbf{w}_t}], \\ &= \max_{\|\mathbf{w}_t\|_2=1} \mathbf{w}_t^H [\mathbf{a}_{(0:N-2)} \mathbf{a}_{(0:N-2)}^H - \kappa^2 \mathbf{A}^T \mathbf{A}^*] \mathbf{w}_t, \end{aligned} \quad (26)$$

where the constraint  $\|\mathbf{w}_s\|_2 = 1$  is chosen to obtain a finite solution. Using the method of Lagrange multipliers, it can be shown that the desired temporal weight vector is the eigenvector corresponding to the maximum eigenvalue of the  $(N-1) \times (N-1)$  matrix  $[\mathbf{a}_{(0:N-2)} \mathbf{a}_{(0:N-2)}^H - \kappa^2 \mathbf{A}^T \mathbf{A}^*]$ . This formulation yields a spatial weight vector of length  $(N-1)$ . The loss of one DOF represents the subtraction operation in defining the entries of  $\mathbf{A}$ .

Analogous to the spatial adaptive weights, the temporal weight vector  $\mathbf{w}_t$  is the eigenvector corresponding to the largest eigenvalue of the  $(M-1) \times (M-1)$  matrix

$[\mathbf{b}_{(0:M-2)}\mathbf{b}_{(0:M-2)}^H - \kappa^2\mathbf{B}^T\mathbf{B}^*]$ , where  $\mathbf{b}_{(0:M-2)}$  is the vector of the first  $(M-1)$  entries of the temporal steering vector defined by Eqn. (14) and  $\mathbf{B}$  is the  $N \times (M-1)$  matrix

$$\mathbf{B} = \begin{bmatrix} \mathbf{X}_{00} - z_t\mathbf{X}_{01} & \mathbf{X}_{01} - z_t\mathbf{X}_{02} & \dots & \mathbf{X}_{0(M-2)} - z_t\mathbf{X}_{0(M-1)} \\ \mathbf{X}_{10} - z_t\mathbf{X}_{11} & \mathbf{X}_{11} - z_t\mathbf{X}_{12} & \dots & \mathbf{X}_{1(M-2)} - z_t\mathbf{X}_{1(M-1)} \\ \vdots & \vdots & \vdots & \vdots \\ \mathbf{X}_{(N-1)0} - z_t\mathbf{X}_{(N-1)1} & \mathbf{X}_{(N-1)1} - z_t\mathbf{X}_{(N-1)2} & \dots & \mathbf{X}_{(N-1)(M-2)} - z_t\mathbf{X}_{(N-1)(M-1)} \end{bmatrix} \quad (27)$$

The length  $NM$  space-time adaptive weight vector, for look angle  $\phi_t$  and look Doppler  $f_t$  is then given by

$$\mathbf{w}(\phi_t, f_t) = \begin{bmatrix} \mathbf{w}_t \\ 0 \end{bmatrix} \otimes \begin{bmatrix} \mathbf{w}_s \\ 0 \end{bmatrix} \quad (28)$$

The zeros appended to the spatial and temporal weight vectors represent the lost DOF in space and time.

The parameter  $\kappa$  above sets a trade off between mainbeam gain and interference suppression. By changing the value of this parameter, it is possible to emphasize one or the other term. In determining the spatial weights, choosing  $\kappa = 0$  eliminates the interference term leaving the largest eigenvalue equal to  $\|\mathbf{a}_{(0:N-2)}\|_2^2 = (N-1)$  with the corresponding eigenvector  $\mathbf{w}_s = \mathbf{a}_{(0:N-2)} / \|\mathbf{a}_{(0:N-2)}\|_2$ . Therefore, as  $\kappa \rightarrow 0$  the  $D^3$  weight vector approaches the non-adaptive steering vector used in pulse-Doppler processing.

On the other hand, if  $\kappa$  is chosen to be large, the role of the gain term  $G$  is negligible and the weight vector is dependent on the interference terms only. This leads to emphasis on the suppression of interference at the expense of mainbeam gain. In this case, the look direction plays a limited role through the term  $z_s$  and the weight vector may vary significantly by range cell.

Note that the adaptive weight vector in Eqn. (28) is obtained using data from the *primary range cell only*. There is no estimation of a covariance matrix and no correlation information required to obtain the adaptive weights. This property gives direct data domain processing its greatest advantage and its greatest disadvantage. The lack of an estimation of correlation allows use of  $D^3$  processing in severely non-homogeneous situations. However, ignoring correlation information limits its ability to suppress correlated interference. A hybrid method to overcome this drawback and combine the benefits of statistical and non-statistical ( $D^3$ ) processing will be described in Section 3.1.

### 2.5.1 Performance of $D^3$ Processing in Non-homogeneous Interference

This section presents a simulation to illustrate the advantages and disadvantages of  $D^3$  processing. This simulation includes the effects of clutter, barrage noise jammers, white noise and a discrete interferer. Table 1 lists the parameters used in the example. The jammer and discrete interferer powers are referenced to the noise level. The clutter power is fixed by the transmit power and the assumed land reflectivity. The clutter and jammers represent correlated interference because these two interference sources are homogeneous across all range cells. Note that the discrete interferer is within the target range cell only, with an offset from the look direction in angle but not Doppler. Matching the non-homogeneity to the target in one domain makes it more difficult for the  $D^3$  algorithm to suppress the non-homogeneity.

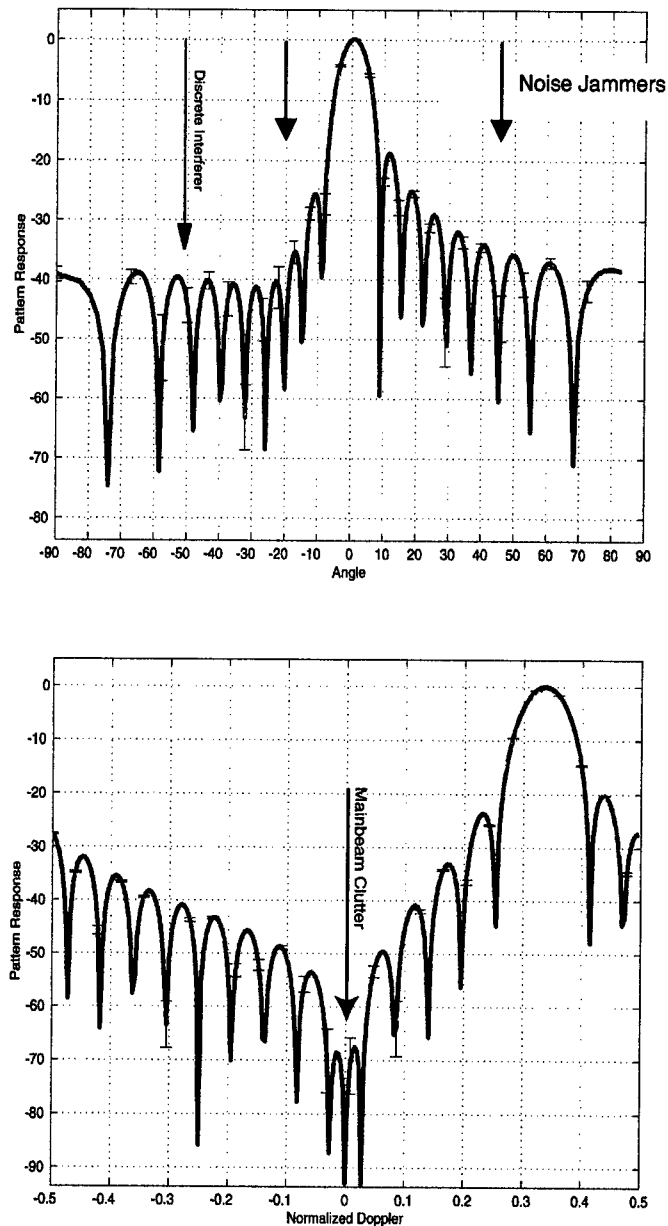
**Table 1: Parameters for example using simulated data**

<i>Parameter</i>	<i>Value</i>	<i>Parameter</i>	<i>Value</i>
Elements ( $N$ )	18	Pulses ( $M$ )	18
Element Spacing	$0.5\lambda$	Pulse repetition frequency	300 Hz
Array Transmit Pattern	Uniform	Uncompressed pulse width	400 $\mu$ s
Mainbeam Transmit Azimuth	0 deg	Transmit power	400kw
Backlobe attenuation	30	Land reflectivity	-3.0dB
Jammer azimuth angles	[-20° 45°]	Jammer powers	[40 dB 40 dB]
Target normalized Doppler ( $f_t$ )	1/3	Jammer Elevation angles	[0° 0°]
Doppler of interferer	1/3	Interferer power	40 dB
Angle of interferer	-51°	Thermal noise power	Unity
$\beta$ (Clutter slope)	1	Number of clutter patches	361

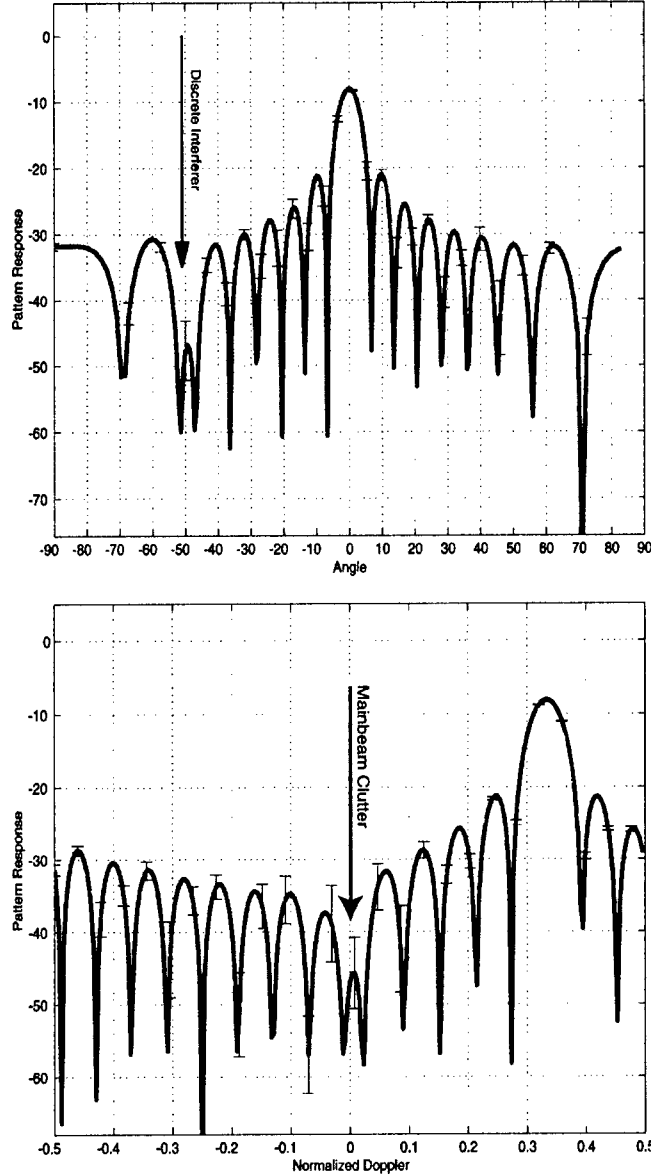
The adapted beam pattern plots presented in this report are the mean patterns over 200 independent realizations. Vertical bars represent the standard deviation over these 200 trials. This method was required because the  $D^3$  algorithm is non-statistical and based solely on a single data set/realization. Operating with the known covariance matrix to obtain an ideal pattern, as possible in statistical algorithms, is not an option.

Figure 20 illustrates the antenna patterns along the target azimuth and Doppler for the JDL algorithm. In the angle plot, note the high sidelobe in the direction of the discrete interferer. The discrete interferer is within the primary range cell and so does not contribute to the covariance matrix estimate and therefore *cannot* be nulled by a purely statistical algorithm such as JDL. However, the angle plot shows the JDL algorithm does

place deep nulls in the direction of the white noise jammers at  $-20^\circ$  and  $45^\circ$ . The Doppler plot shows the deep null placed at zero Doppler frequency corresponding to mainbeam clutter. These two figures illustrate the effectiveness of the JDL algorithm in suppressing correlated interference such as jamming and clutter. However, they also illustrate the inability of a purely statistical algorithm to suppress point non-homogeneities (discretes).



**Figure 20: JDL Antenna Patterns at Target Doppler and Azimuth  
(a) Angle Pattern (b) Doppler Pattern**



**Figure 21: Direct Data Domain Patterns at Target Doppler and Azimuth  
(a) Angle Pattern (b) Doppler Pattern**

Figure 21 plots the antenna patterns resulting from the implementation of the two-dimensional  $D^3$  algorithm. The angle plot shows that the  $D^3$  algorithm places a null in the direction of the discrete interferer. The adapted spatial beam pattern shows a distinct null in the direction of the discrete interferer at  $-51^\circ$ , i.e. the algorithm is effective in countering a discrete interferer within the range cell of interest. However, the figure also illustrates the limitations of the  $D^3$  algorithm. The nulls in the direction of the jammers are not as deep as in the case of JDL. The Doppler plot shows a shallow null in the direction of the mainbeam clutter. In summary,  $D^3$  algorithms do not suppress correlated interference as well as statistical algorithms, however they are an excellent processing technique to deal



with non-homogeneities. Later in this report, we present results from combining the benefits of  $D^3$  and statistical algorithms.

### 3.0 GMTI-STAP Status

This section details the on-going research undertaken with the support of DARPA. The research presented here is a continuation of the work presented in Section 2.0 addressing some of the issues raised. We developed a hybrid algorithm combining non-statistical and statistical adaptive processing and use this algorithm to develop the simplest formulation for a comprehensive, practical, approach to STAP. This formulation accounts for all the real world effects listed in Section 2.0.

Section 2.5 discusses non-statistical adaptive processing in non-homogeneous environments, pointing out both the advantages and drawbacks of such an approach. Here we present a unique formulation combining the benefits of non-statistical and statistical processing. This hybrid algorithm, presented in section 3.1, is a two-stage algorithm combining the two approaches. The issues of non-homogeneous data, non-homogeneity detection and the hybrid algorithm lead to a formulation using *Knowledge Based STAP* (KB-STAP). Section 3.2 presents the KB-STAP concept and simplest KB-STAP formulation. The examples presented in this section show the huge improvements in performance over traditional STAP algorithms and prove the importance of the issues raised in this report. Section 3.3 presents further enhancements to KB-STAP, incorporating map data to inform the decision making process within the knowledge base.

### 3.1 Hybrid (D3/JDL) STAP

Performance degradation of STAP algorithms due to non-homogeneous data occurs in two forms. In one form the secondary data is not i.i.d., leading to an inaccurate estimate of the covariance matrix. For example, the clutter statistics in urban environments fluctuate rapidly with range. To minimize the loss in performance due to non-homogeneous sample support, a NHD may be used to identify secondary data cells that do not reflect the statistical properties of the primary data. These data samples are then eliminated from the estimate of the covariance matrix.

The second form of performance loss is due to a discrete non-homogeneity within the primary range cell. For example, a large target within the test range cell but at a different angle and/or Doppler appears as a false alarm at the look angle-Doppler domain. Other examples include a strong discrete non-homogeneity, such as a large building (corner reflector), in the primary range cell. These false alarms appear through the sidelobes of the adapted beam pattern. The secondary data cells do not carry information about the discrete non-homogeneity and hence a statistical algorithm cannot suppress discrete (uncorrelated) interference within the range cell under test. The example presented in Section 2.5.1 illustrated the impact of such a non-homogeneity.

The inability of statistical STAP algorithms to counter non-homogeneities in the primary data motivates research in the area of non-statistical  $D^3$  algorithms, such as that described in Section 2.4. These algorithms use data from the range cell of interest only, eliminating the sample support problems associated with statistical approaches.

The main contribution of this section is the introduction of a two-stage hybrid STAP algorithm combining the benefits of both non-statistical and statistical methods. The hybrid approach uses the non-statistical algorithm of Section 2.4 as a first-stage filter to suppress discrete interferers present in the range cell of interest. This first stage serves as an *adaptive transform* from the space-time domain to the angle-Doppler domain and is followed by JDL processing in the second stage. The adaptive transform replaces the steering vector based non-adaptive transform used in Section 2.3. The second stage is designed to filter out the residual correlated interference [15].

### 3.1.1 Two-Stage Hybrid Algorithm

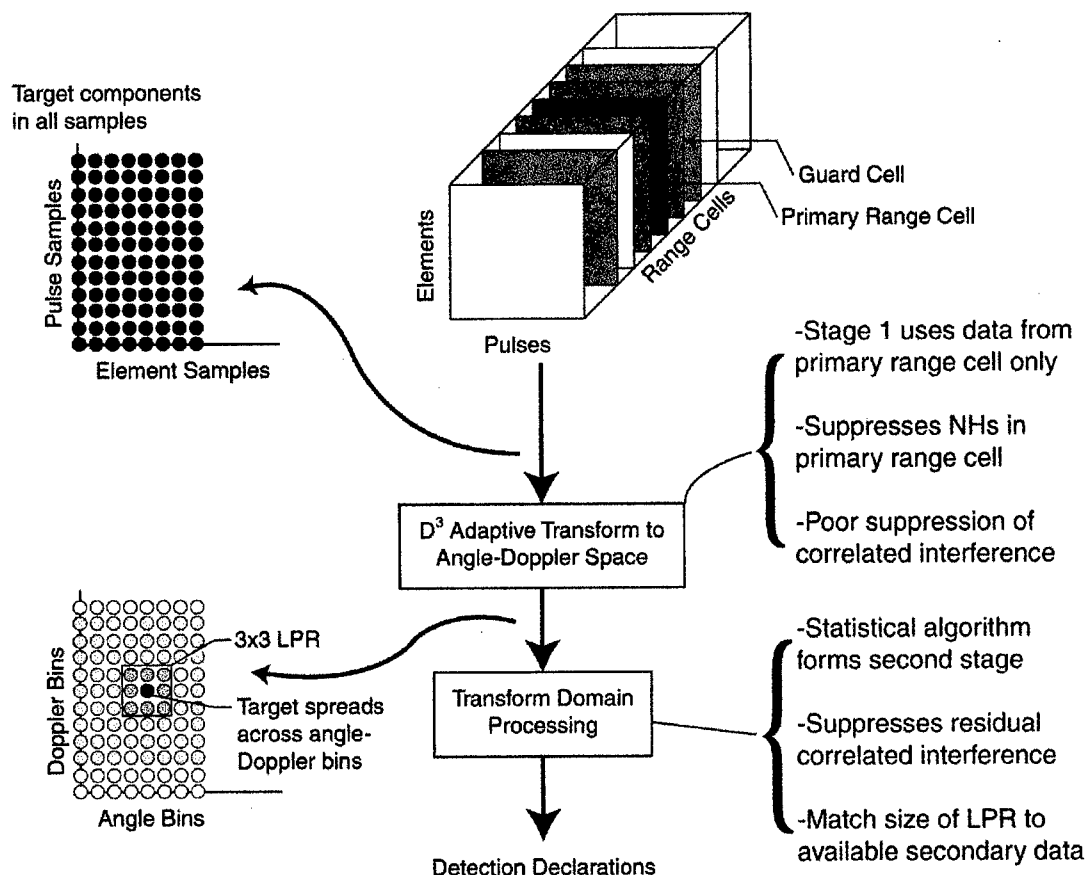


Figure 22: Block diagram of the Two-Stage Hybrid Algorithm

Consider the general framework of any STAP algorithm. The algorithm processes received data to obtain a complex weight vector for each range bin and each look angle/Doppler. The weight vector then multiplies the primary data vector to yield a complex number. The process of obtaining a real scalar from this number for threshold comparison is part of the post-processing and not inherent to the algorithm itself. The adaptive process therefore *estimates the signal component in the look direction* and hence the adaptive weights can be viewed in a role *similar to the non-adaptive steering vectors*, used to transform the space-time data to the angle-Doppler domain.

The JDL processing algorithm begins with a transformation of the data from the space-time domain to the angle-Doppler domain. This is followed by statistical adaptive processing within a LPR in the angle-Doppler domain. The hybrid approach uses the  $D^3$  weights, replacing the non-adaptive steering vectors used earlier. By choosing the set of look angles and Dopplers to form the LPR, the  $D^3$  weights perform a function analogous to the non-adaptive transform. As shown in Figure 22, the  $D^3$  algorithm serves as a first stage *adaptive* transformation from the space-time to the angle-Doppler domain.

JDL statistical processing in the angle-Doppler domain forms the second stage of adaptive processing to filter the residual correlated interference. The  $D^3$  algorithm is used repeatedly with the  $\eta_a$  look angles and the  $\eta_d$  look Doppler frequencies to form the LPR. The space-time data is transformed to the LPR in the angle-Doppler domain using these adaptive weights. Using the  $D^3$  weights from Eqn. (28), the transformation matrix of Eqn. (20) in Section 2.3 for  $(\phi_{-1}, \phi_0, \phi_1; \eta_a = 3)$  and three Doppler bins  $(f_{-1}, f_0, f_1; \eta_d = 3)$  is now given by the  $MN \times 9$  matrix

$$\mathbf{T} = \begin{bmatrix} \mathbf{w}(\phi_{-1}, f_{-1}) & \mathbf{w}(\phi_{-1}, f_0) & \mathbf{w}(\phi_{-1}, f_1) \\ \mathbf{w}(\phi_0, f_{-1}) & \mathbf{w}(\phi_0, f_0) & \mathbf{w}(\phi_0, f_1) \\ \mathbf{w}(\phi_1, f_{-1}) & \mathbf{w}(\phi_1, f_0) & \mathbf{w}(\phi_1, f_1) \end{bmatrix} \quad (29)$$

This adaptive transformation is noninvertible, resulting in some information loss. However, this information loss may be beneficial. The hybrid algorithm takes advantage of this loss to suppress discrete interferers within the range cell of interest. The advantages associated with the JDL algorithm, such as in reduction in the required secondary data support, carry over to the hybrid algorithm.

The same transformation matrix  $\mathbf{T}$  is used to transform the primary and secondary data to the angle-Doppler domain. Furthermore, the steering vector  $\mathbf{s}$  is also transformed to the angle-Doppler domain using this transformation matrix in conjunction with Eqn. (21). Unlike the JDL algorithm, this transformation matrix changes from range cell to range cell. The hybrid algorithm therefore has a significantly higher computation load than the JDL algorithm. The hybrid algorithm forms the adaptive transformation matrix as given by Eqn. (29) for each range cell and then transforms this primary and *associated*

secondary data to the angle-Doppler domain. This process is repeated for each range cell.

### 3.1.2 Example 1: Simulated Data

The first example uses the same data as presented in Section 2.5.1 to illustrate the performance of the  $D^3$  method. There it was shown that the  $D^3$  algorithm can suppress a discrete interference source well, but does not do as well against correlated interference such as white noise jamming and clutter. This example shows the performance of the hybrid algorithm in the same case.

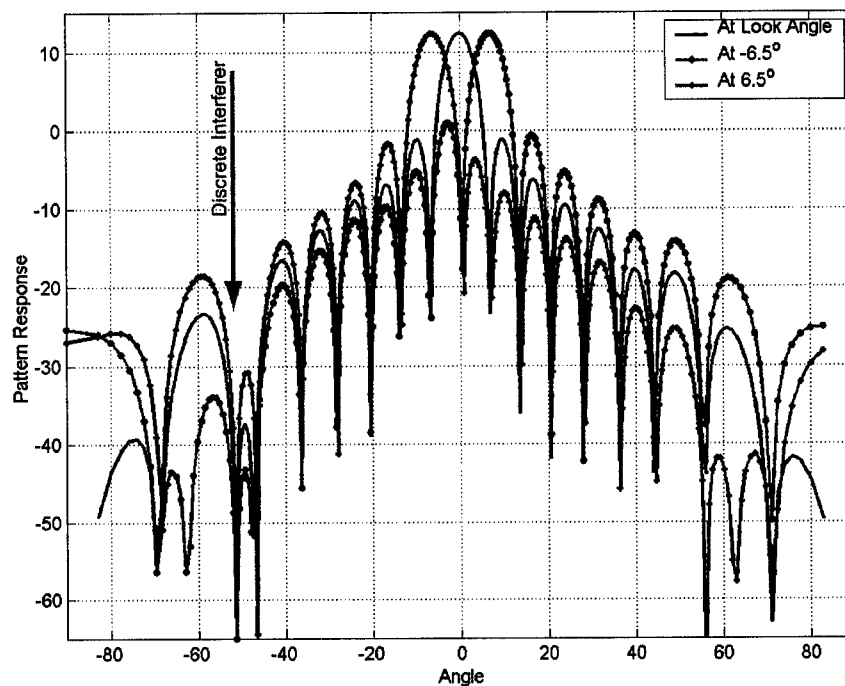
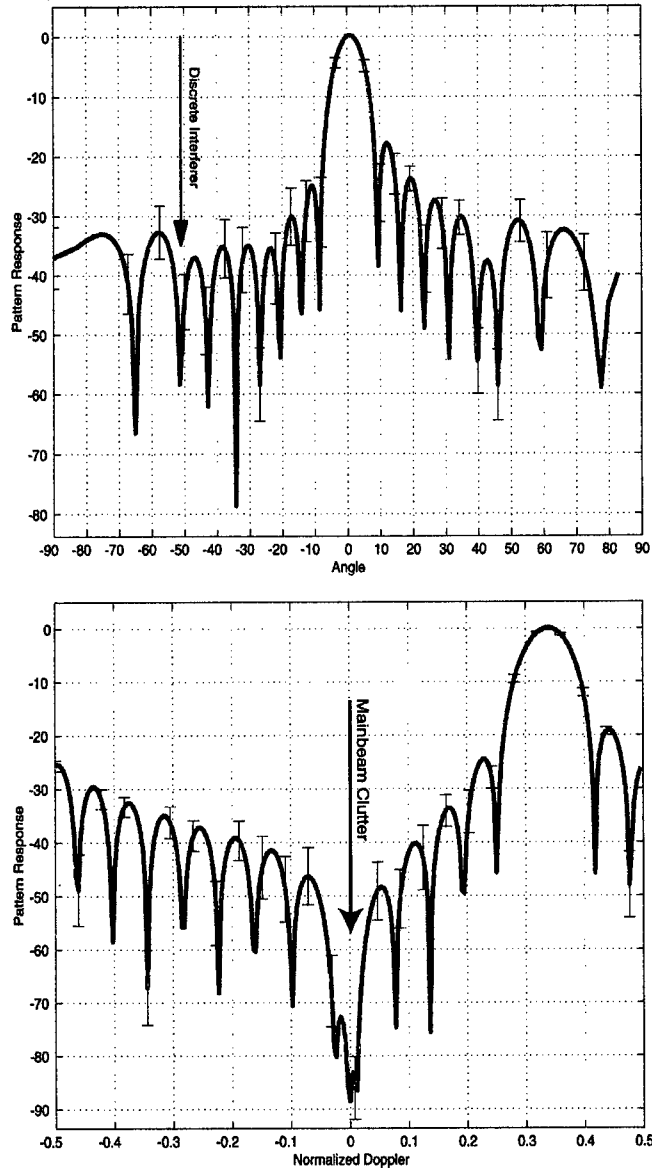


Figure 23: Three  $D^3$  spatial beams used to form LPR

This example uses 3 angle bins and 3 Doppler bins, i.e.  $3 \times 3$  LPR. The emphasis parameter  $\kappa$  is chosen to be  $(NM)^{1/2}$ . Figure 23 plots the spatial beam patterns associated with the three beams used to form the LPR in angle-Doppler domain. Note that the three beams are separated by a chosen beamwidth of  $6.5^\circ$ . All three patterns show a null in the direction of the discrete interferer at angle  $-51^\circ$ . These beams illustrate the benefits of using the  $D^3$  algorithm as the first stage. The algorithm suppresses discrete interference and the data transformed the angle-Doppler domain is free of the effects of discretely in the spatial sidelobes.

Figure 24 plots the antenna beam patterns resulting from the use of the hybrid algorithm. The figure shows that the hybrid algorithm combines the advantages of both statistical and non-statistical adaptive processing. The adapted angle pattern shows deep nulls at  $-21^\circ$ ,  $45^\circ$ , and  $-51^\circ$ , the directions of the two jammers *and the discrete interferer*. Furthermore, the adapted pattern has a deep null at  $\omega=0$  resulting in effective nulling of the mainbeam clutter. The hybrid algorithm therefore suppresses correlated interference such as clutter and jamming *and uncorrelated interference such as the strong interferer* in the primary range cell.



**Figure 24: Hybrid Algorithm Patterns at Target Doppler and Azimuth**

### 3.1.3 Applying the Hybrid Algorithm to Measured Data

This section presents two examples of the application of the hybrid algorithm to measured data. The examples use data from the MCARM database. The examples use two acquisitions (acquisitions 575 and 152 on flight 5) to illustrate the suppression of discrete interference in measured data.

Before the hybrid algorithm can be applied to the MCARM database, array effects must be accounted for. The  $D^3$  method was developed in Section 2.5.1 for an equispaced, linear array of point sensors. This allowed for the assumption of no mutual coupling between the elements and that, for each pulse, the target signal advances from one element to the next by a constant spatial multiplicative factor  $z_s$ . This, in turn, allowed for the crucial assumption of the elimination of the target signal in the entries of the interference matrix.

The MCARM antenna is an array of 22 elements arranged in a rectangular 2 x 11 grid. For a rectangular array these assumptions are invalid. Furthermore, as shown in Section 2.3.1, a real array is affected by mutual coupling and the spatial steering vector must be measured. Figure 13 plots an example of the measured steering vectors provided with the MCARM database.

Here we compensate for the mutual coupling using the measured steering vectors (similar to the approach used in Section 2.2 for the JDL algorithm). Equation (13) indicates that the spatial steering vector at broadside ( $\phi = 0$ ) is given by  $\mathbf{a}(\phi = 0) = [1 \ 1 \dots 1 \ 1]^T$ . In the absence of mutual coupling, this steering vector at broadside is valid for arrays in *any* configuration. The approach then is to artificially rotate all the data, using the measured spatial steering vector, to force the look direction to broadside. This compensates for the rectangular array configuration and the mutual coupling associated with the look direction. The rotation is achieved by an entry-by-entry division of the received voltages at the array level with the measured spatial steering vector corresponding to the look direction. Using pseudo-MATLAB<sup>®</sup> notation, this operation can be represented by

$$\hat{\mathbf{x}}(m) = \mathbf{x}(m) ./ \mathbf{a}_m(\phi_l), \quad (30)$$

where  $\mathbf{x}(m)$  represents the  $N$  returns from the  $m^{\text{th}}$  pulse in a CPI and  $\mathbf{a}_m(\phi_l)$  represent the measured steering vector corresponding to the look direction  $\phi_l$ . This operation is repeated for all pulses in all range bins.

The division operation of Eqn. (30) forces the effective spatial steering vector for any look direction to be  $\mathbf{a}(\phi = 0) = [1 \ 1 \dots 1 \ 1]^T$ , equivalent to broadside in an ideal array. The hybrid method as developed above is applied to the ‘rotated’ data with broadside as the look direction.

### 3.1.4 Example 2: Injected Target in MCARM Data

In this example, a discrete non-homogeneity is introduced into the data by adding a strong fictitious target at a single range bin, but not at the look angle-Doppler. Two cases are considered within this example; no injected target and an injected weak target. The first case illustrates the suppression of the discrete non-homogeneity. In the second case, a weak target is injected at the same range bin as the non-homogeneity, but at the look angle and Doppler. This case illustrates the ability of the hybrid algorithm to detect weak targets in the presence of strong discrete non-homogeneities. The data is the same as used earlier in this report to illustrate the performance of the JDL algorithm. In this case, only 22 of the 128 pulses in the CPI are used, i.e.  $N=22$ ,  $M=22$ . The value of the emphasis parameter is  $\kappa = (NM)^{3/2}$ .

The details of the injected non-homogeneity and weak target are shown in Table 2.

**Table 2: Parameters for injected non-homogeneity and target in MCARM Data**

Parameter	Non-homogeneity	Target
Amplitude	0.0241	0.000241
Angle bin	35	65 (broadside)
Doppler bin	-3	-2
Range bin	290	290

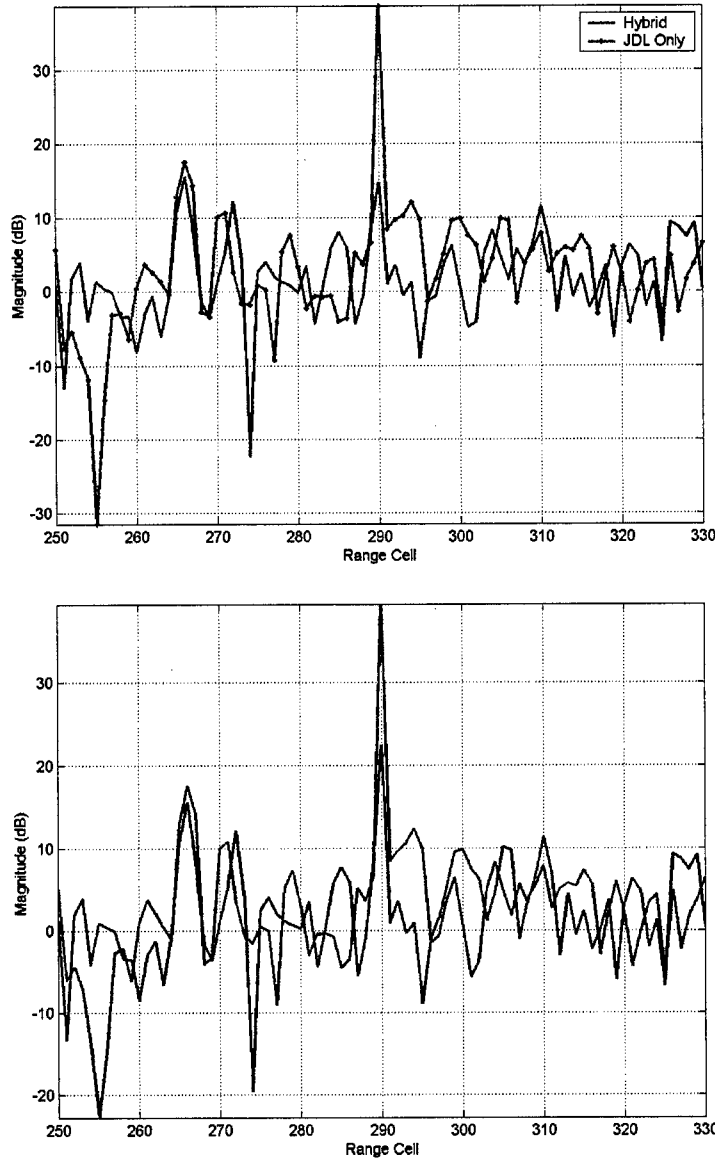


**Figure 25: Performance of Hybrid algorithm in countering non-homogeneities: Injected Target**  
**(a) With Non-homogeneity, No target (b) With non-homogeneity, With target**

The hybrid algorithm is applied to the data from the range bin with the non-homogeneity and surrounding range bins. The output MSML statistic from the second stage of the hybrid algorithm is plotted as a function of range. In this example, five Doppler bins and five angle bins form the LPR for both the JDL algorithm and the second stage of the hybrid algorithm. One hundred secondary data vectors are used to estimate the  $25 \times 25$  covariance matrix.

For the case without an injected target, Figure 25(a) compares the output from the JDL algorithm with the output of the hybrid algorithm. As can be seen, the JDL algorithm indicates the presence of a large target in the look direction (angle bin 65). This is because the large non-homogeneity at angle bin 35 and Doppler bin  $-3$  is not suppressed



by the statistical algorithm, leading to false alarms at the look direction. On the other hand, the hybrid algorithm shows no target at broadside. The non-homogeneity is suppressed in the first  $D^3$  stage and residual clutter is suppressed in the second JDL stage.

A synthetic target injected at the look direction and Doppler illustrates that sensitivity of the hybrid algorithm to weak targets. The parameters of the weak target are listed in Table 2. Figure 25(b) compares the output of the two algorithms in the case of a strong non-homogeneity and a weak target. The JDL algorithm again shows the presence of a strong target in the look direction. However from Figure 25(a), we know that the strength of the statistic is caused by the non-homogeneity. On the other hand, the plot for the hybrid algorithm shows the statistic at the target range bin is 6.9 dB above the next highest peak.

This example shows that the hybrid algorithm may be use to detect a weak target in the presence of a discrete non-homogeneity within the range cell of interest. This is a unique capability compared to all other STAP approaches.

### 3.1.5 Example 3: MTS Tones in the MCARM Data:

Certain acquisitions within the MCARM database include signals from a moving target simulator (MTS) at known Doppler shifts. One of these acquisitions was used in Section 2.3.3 to illustrate the benefits of accounting for array effects. In acquisition 152 on flight 5, the MTS tones occur in angle bin 59. In this example, the look direction is set to angle bin 85 for a mismatch (with the MTS direction) and the JDL and hybrid algorithms are applied to the same acquisition. For this look direction, the MTS tones at angle bin 59 act as strong targets at a different angle bin, i.e. discrete non-homogeneities. As in Example 1, two cases are considered; no injected target and a weak injected target. The first case illustrates the suppression of the MTS tones acting as discrete, strong non-homogeneities. The second case illustrates the sensitivity of the hybrid algorithm to weak targets. This example uses all 128 pulses in the CPI, i.e.  $N = 22$ ,  $M = 128$ . The emphasis parameter for the direct data domain method is set to a large value of  $\kappa = (NM)^{3/2}$ .

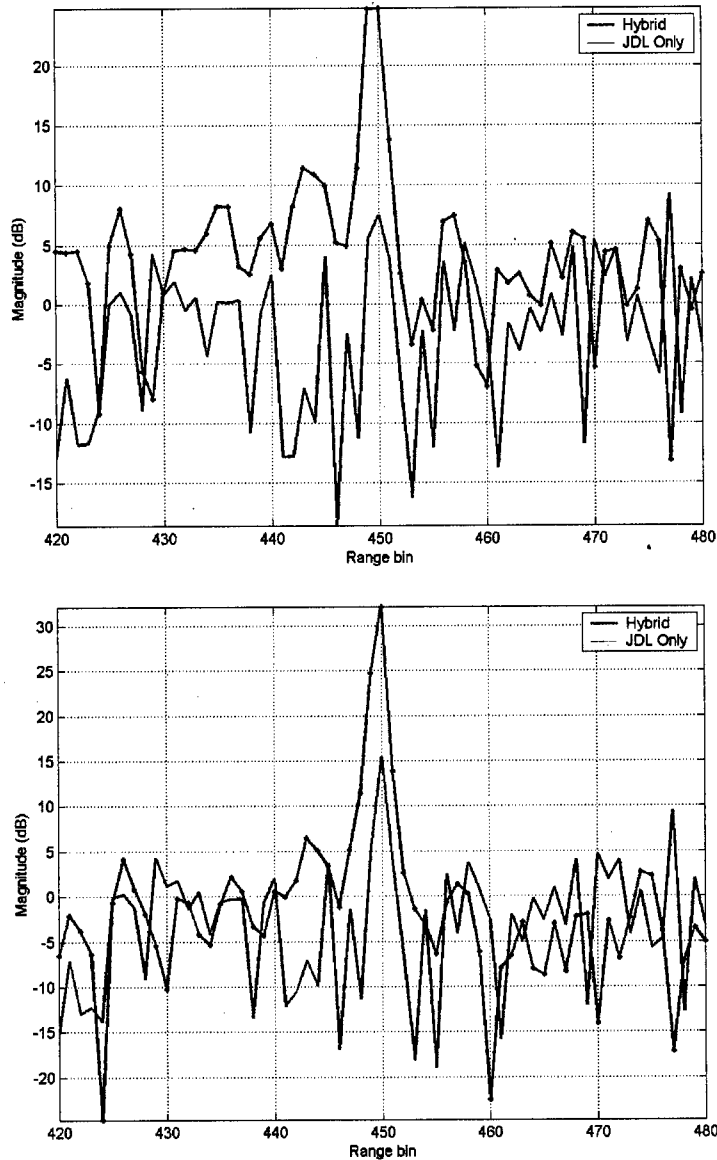


**Figure 26: Performance of Hybrid algorithm in countering non-homogeneities: MTS Data (a) With Non-homogeneity, No target (b) With non-homogeneity, With target**

In this acquisition, the MTS tones are in range bin 449-450 with the strongest tone at a Doppler corresponding to bin -53 and angle bin 59. The example focuses on the suppression of this tone. Figure 26(a) plots the MSMI statistic of the two algorithms for the case without any artificial injected targets. The JDL algorithm detects a large target at range bins 449 and 450. This false alarm is due to the strong MTS tone at angle bin 59 even though the look direction is set at angle bin 85. The hybrid algorithm, however, suppresses the strong MTS tone, showing no activity at range bins 449 and 450.

Figure 26(b) plots the results of using the two algorithms to detect a weak target injected into range bin 450. The parameters of the weak target are; magnitude: 0.0001,

Doppler bin: -53, angle bin: 85. This weak target is easily detected by the hybrid algorithm with the statistic at the target range bin 9.8 dB above the next highest peak.

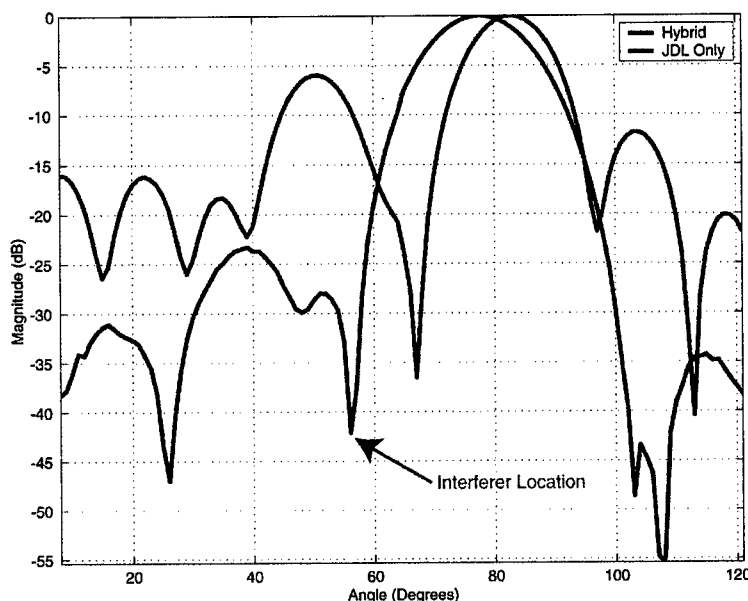


**Figure 27: Beam Pattern associated with the Hybrid and JDL methods**

The beam patterns associated with the two algorithms illustrate the improvement in using the  $D^3$  algorithm as the first stage of a two-stage hybrid method. Figure 27 plots the spatially adapted beam pattern at the look Doppler frequency for the JDL and hybrid algorithms. The plot for the hybrid algorithm shows the deep null in the adapted pattern of the hybrid algorithm near angle bin 59 while the JDL pattern does not show such a null. In applying the JDL algorithm to the MCARM data acquisition with MTS tones, the strong tones leak through the sidelobes of the adapted pattern, leading to false alarms.

### 3.1.6 Summary

This section presented the hybrid algorithm, developed specifically for the non-homogeneous data case. Statistical algorithms cannot suppress discrete non-homogeneities because the secondary data possesses no information regarding such interference. The  $D^3$  method, presented earlier, however can suppress such discrete interference. However, performance of  $D^3$  algorithms in homogeneous interference scenarios is inferior to traditional statistical STAP algorithms. Each of these two approaches to STAP has its own area of application.

The proposed two-stage hybrid algorithm alleviates this drawback by implementing a second stage of statistical processing after using the  $D^3$  algorithm as an adaptive transform to the angle-Doppler domain. This algorithm combines the advantages of both the statistical and non-statistical approaches. The  $D^3$  method is particularly effective at

countering non-homogeneous interference. The statistical STAP algorithm then improves on the suppression of the residual correlated interference.

Even with *ad hoc* compensation for mutual coupling, the hybrid algorithm shows a significant improvement over statistical methods in suppression discrete non-homogeneities. We anticipate a true evaluation of the mutual coupling would improve the performance of the hybrid algorithm.

### 3.2 Knowledge Based Processing

The field of Space-Time Adaptive Processing has received much interest in the past 30 years. The sum total of the research is extensive, with several classes of algorithms, some practical and others not so practical. In addition, interesting new algorithms [16] and algorithms that address particular interference situations [17] are being continually developed. What is clear is that there is no single algorithm that is optimal in all interference scenarios. In a relatively homogeneous scene, an algorithm such as FA-STAP may be best, while in a non-homogeneous scene JDL may be the best or even possibly the  $D^3$  algorithm in an extremely non-homogeneous case. All statistical algorithms require the estimation of a covariance matrix. In a non-homogeneous scene, the choice of the secondary data has a huge impact on the performance of the algorithm. It is essential that in a real world situation the secondary data be chosen properly.

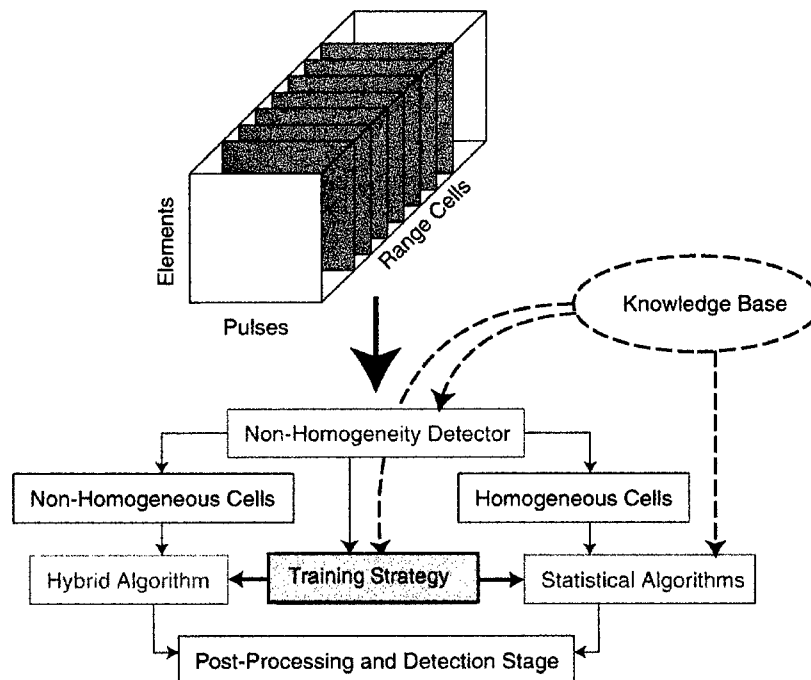


Figure 28: Knowledge Based Space-Time Adaptive Processing (KB-STAP)

This research therefore heads towards the concept of *Knowledge Based STAP* (KB-STAP). KB-STAP [18] chooses the best of several possible STAP algorithms for detection with knowledge-based control of algorithm parameters and selection of secondary data using NHDs. The basic elements of a comprehensive KB-STAP formulation are shown in Figure 28. Any comprehensive algorithm for practical implementation of STAP requires at least three elements: a non-homogeneity detector to separate the received data into homogeneous and non-homogeneous sectors, a statistical algorithm for use within the homogeneous sectors and a hybrid algorithm for use within the non-homogeneous sector. This section presents the performance improvements possible using such a combined scheme [19].

The combined approach is tested using data from the MCARM database. As described earlier, each CPI comprises the data corresponding to 22 digitized channels and 128 pulses at a PRF of 1984 Hz. The datacube comprises 630 range cells, sampled at  $0.8\mu\text{s}$ . Each range bin, therefore, corresponds to 0.075miles. The array operates at a center frequency of 1.24GHz. Included with each CPI is information regarding the position, aspect, velocity and mainbeam transmit direction. This information is used to correlate target detections with ground features.

The example illustrates the issues addressed in this report, namely non-homogeneities and the use of the appropriate processing algorithm in appropriate portions of the radar data cube. Non-homogeneity detection is accomplished using JDL assuming homogeneous data. Any range bin with a statistic above a chosen threshold is considered non-homogeneous. The statistical algorithm is JDL again, though in the second stage only homogeneous data is used in the sample support. The hybrid algorithm also uses only homogeneous data for sample support in second stage.

This example uses data from acquisition 575 on flight 5. While taking this acquisition the radar platform was at latitude-longitude coordinates of  $(39.379^\circ, -75.972^\circ)$ , placing the aircraft close to Chesapeake Haven, Maryland, near the Delmarva peninsula. The plane was flying mainly south with velocity 223.78mph and east with velocity 26.48mph. The aircraft location and the transmit mainbeam are shown in Figure 29. The mainbeam is close to broadside. Note that the mainbeam illuminates several major highways.

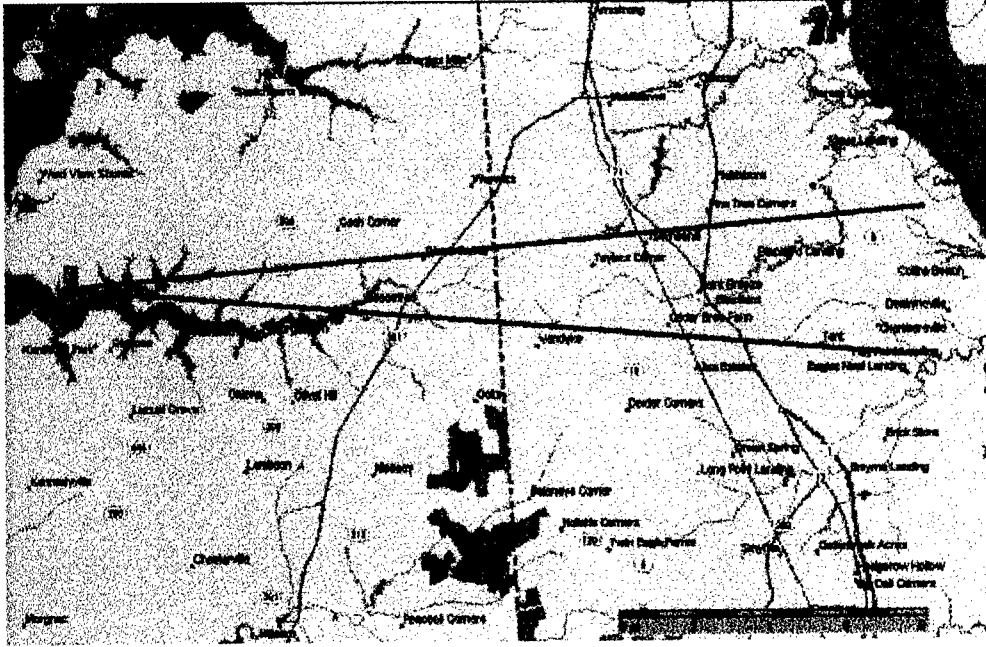


**Figure 29: Location and transmit direction of the MCARM Aircraft during the acquisition**

In addition to the targets of opportunity on the roadways illuminated by the array, we inject two artificial targets at closely spaced range bins to illustrate the effects of non-homogeneities in secondary training data. Based on the measured steering vectors and chosen Doppler shifts the response of the two simulated targets may be calculated. The artificial targets are injected in range bins 290 and 295. In this acquisition the transmit pulse is zero-shifted to range bin 74, i.e. the targets are at ranges of 16.2miles and 16.575miles respectively. The parameters of the injected targets are:

**Table 3: Parameters of the injected targets**

Target 1		Target 2	
Amplitude	$1 \times 10^{-4}$	Amplitude	$1 \times 10^{-3}$
Range bin	290	Range bin	295
Doppler	Bin $-9 \equiv 137.5\text{Hz}$	Doppler	Bin $-9 \equiv 137.5\text{Hz}$
Angle	$1^\circ$	Angle	$1^\circ$

Note that the two targets are at the same Doppler frequency and the second target is 20dB stronger than the first.

This example uses 3 angle bins and 3 Doppler bins (a  $3 \times 3$  LPR) in all stages of adaptivity, including the JDL-NHD. Thirty-six secondary data vectors are used to estimate the  $9 \times 9$  angle-Doppler LPR covariance matrix. In addition, two guard cells are used on either side of the primary data vector. Based on these numbers, without a NHD stage,

range bin 295 would be used as a secondary data vector for detection within range bin 290. The example compares the results of using the JDL algorithm without non-homogeneity detection and the combined approach illustrated in Figure 28.

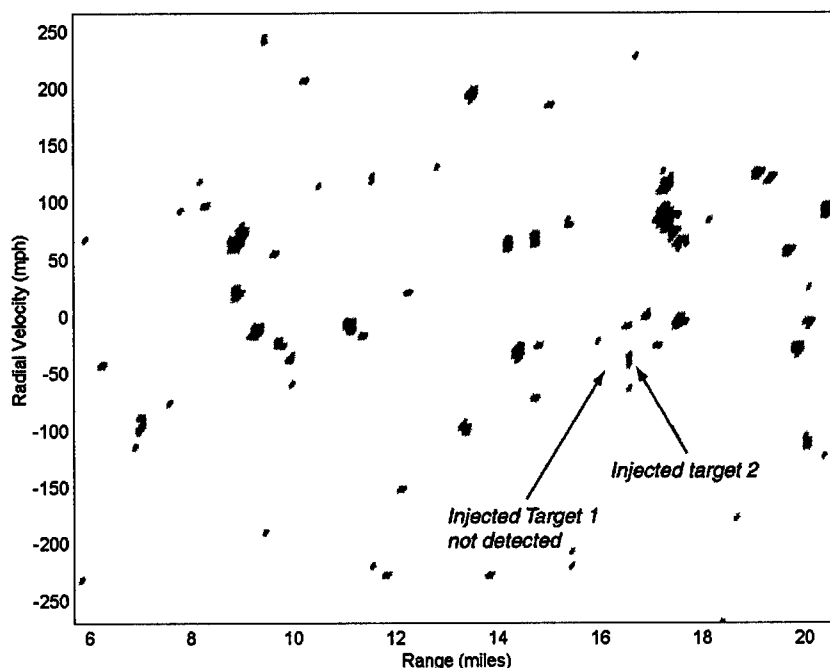


**Figure 30 : JDL Processing without accounting for non-homogeneities**

Figure 30 presents the results of using the JDL algorithm without any attempt to remove non-homogeneities from the secondary data support. The range-Doppler plot is of the MSMI statistic after applying a threshold. In producing this figure, a threshold of 40 is used, i.e. any Doppler-range bin with a MSMI statistic greater than 40 (amplitude not in dB) is said to contain a target while any Doppler-range bin with a statistic below 40 is declared target free. The plot is for adaptive processing between range bins 150 and 350, i.e. ranges between 5.7 and 20.7 miles and all 128 Doppler bins. Due to platform motion the radar is approaching the declared targets at a speed of 26.48mph.

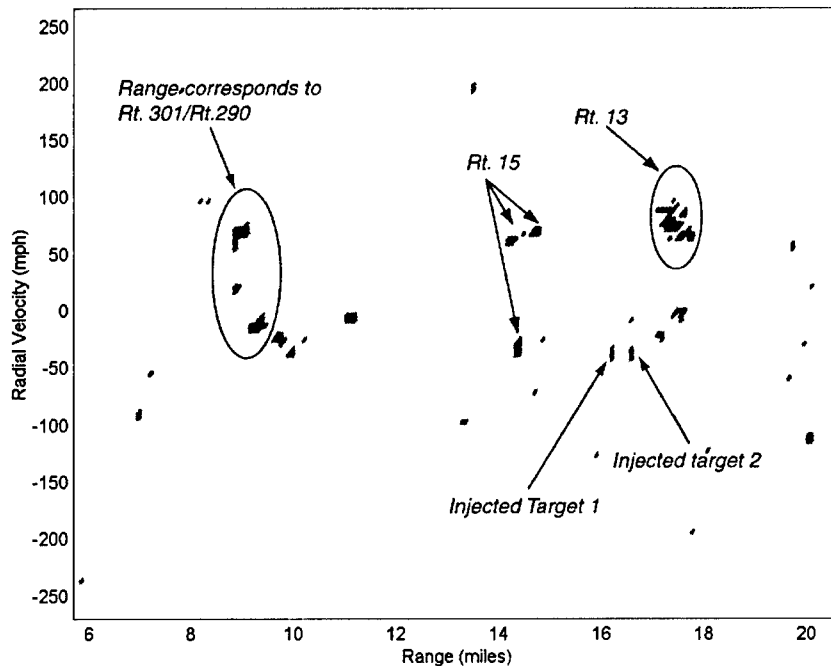
As is shown later, certain range bins that are declared to contain a target can be correlated with the map in Figure 29 as corresponding to roadways. However, this approach results in several false alarms including several at extremely high radial velocities. In addition, the first injected target at range bin 290 is not detected. This is because of the presence of the larger target at range bin 295 in the secondary data when range bin 290 is the primary data.

Figure 30 clearly illustrates the need for a stage to identify non-homogeneities and eliminate them from the secondary data support. Applying STAP to measured data results in several false alarms and the possibility of targets in the secondary data masking weak targets. The processing structure of Figure 28 addresses this need.

In the implementation used in this paper, a JDL-NHD is used to identify non-homogeneous range cells. A range cell is considered to be non-homogeneous if the JDL-MSMI statistic is above 18.52, significantly lower than the threshold of 40 used to generate Figure 30. Assuming Gaussian interference, using 36 secondary data vectors to estimate a  $9 \times 9$  covariance matrix to obtain an MSMI statistic, this threshold corresponds to a false alarm rate of  $P_{fa}=10^{-4}$ . Note that the true false alarm rate using measured data is significantly higher.

The combined algorithm uses JDL processing in those cells declared homogeneous and hybrid processing in those cells declared non-homogeneous. Again, a  $3 \times 3$  LPR is used, both in the JDL algorithm and in the Hybrid algorithm. In the second application of the JDL algorithm in homogeneous range cells, only other homogeneous cells are used for sample support. Within the non-homogeneous cells, a hybrid algorithm is used, i.e. the  $D^3$  algorithm is applied 9 times for 3 angle and 3 Doppler look directions, *using the same primary data*. The angle-Doppler data so obtained is used for further JDL processing. Homogeneous cells are used to obtain sample support for the second stage JDL processing.

Figure 31 shows the result of using the combined approach. Notice the significantly fewer false alarms than in Figure 30 when using a purely statistical algorithm without non-homogeneity detection. In essence the hybrid algorithm is applied to all those range/Doppler bins where the JDL-MSMI statistic is greater than 18.52. The use of the hybrid algorithm suppresses the non-homogeneities thereby significantly reducing the false alarms.



**Figure 31: Combined processing accounting for non-homogeneities**



In addition, the weaker injected target is detected since the stronger target at range bin 295 is eliminated from the sample support for range bin 290. Furthermore, the range bins of most target detections can be directly correlated with the state highways in Maryland and Delaware. Routes 299 and 301 in Maryland are closely spaced at a range of 9.0 and 9.8 miles. Note that the aircraft is moving due east at a speed of 26.48mph. The ground speed of the targets is therefore approximately 50mph towards and away from the aircraft.

The range of the several target detections at the far range shown in the plot, approximately 20miles, is not immediately attributable to Route 9 in Delaware. At broadside, Route 9 is at a range of 21 miles. The detected targets are between 19.4 and 20.4 miles. However, note that Route 9, north-south at broadside curves and has a short east-west section within the 3dB mainbeam. The distance to this section is between 19.1 and 20.6 miles. These targets are detected at these range bins and are present in both Figure 30 and Figure 31.

At a range of approximately 11 miles is a strong detection. Accounting for the aircraft motion, this detection has zero ground velocity. This corresponds to the town of Van Dyke.

This section has presented a comprehensive approach to STAP incorporating the essential elements of a practical scheme: non-homogeneity detection, a statistical algorithm for STAP in homogeneous cells and the hybrid algorithm for STAP in non-homogeneous cells. The example illustrates the importance of these concepts to the GMTI case. This scheme yields huge performance improvements over the traditional STAP algorithm, as applied to real measured data.

The next section presents a formulation to include *a priori* map data to enhance the KB-STAP concept.

### 3.3 MAP-STAP

The formulation presented in the literature uses only one statistical algorithm in homogeneous range cells. To maximize STAP performance, in the long term KB-STAP will choose from several algorithms. The knowledge base processor, using information from diverse sensors, will determine the choice of algorithm to best match the interference scene. For example, in a non-homogeneous scene JDL may be used while in the case of terrain scattered interference, a 3-D spatial/fast-time/slow-time algorithm may be used.

# Knowledge-Based Processing

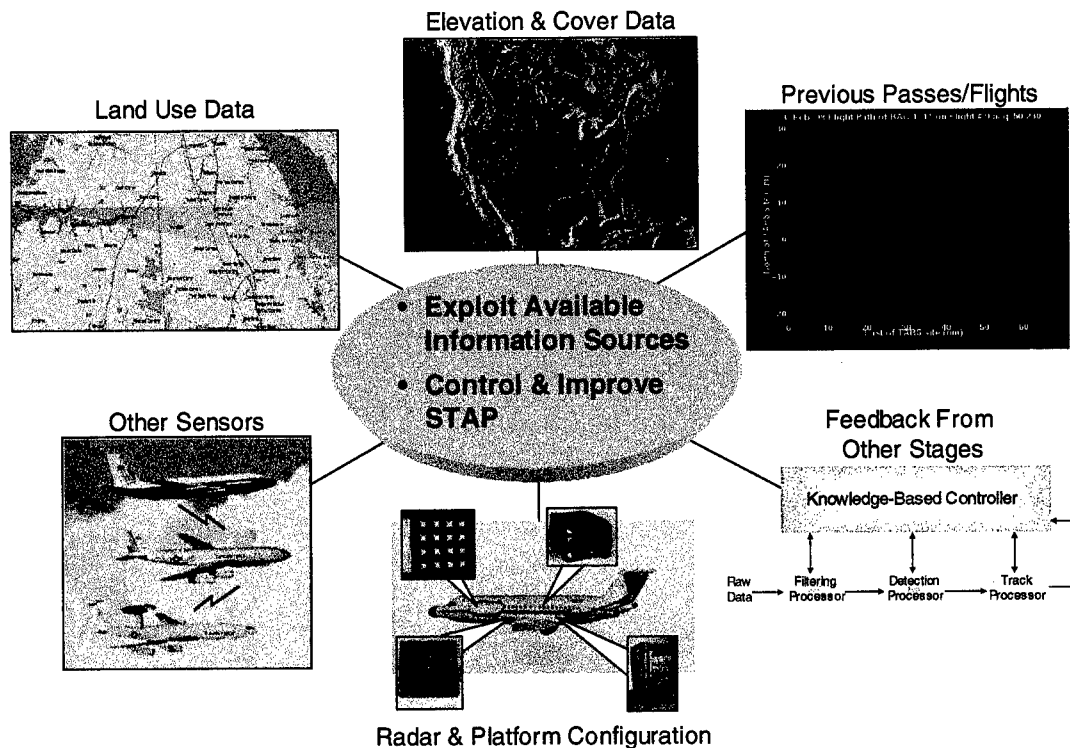


**Figure 32: Sources of Information for KB-STAP**

The KB processor exploits all available information. Figure 32 presents some of the possible knowledge sources: other sensors (e.g. AWACS), land use data, previous passes over the same radar scene and feedback from the tracking and other stages. The open problem is how to fuse all this information together and improve STAP performance. We present the use of one such information source: *a priori* map data.

This philosophy is to determine the terrain illuminated by the radar that best matches the terrain in the primary range cell and at the Doppler of interest, i.e. secondary data that best matches the clutter in the primary range cell. The best source of this information is maps. Using maps to choose the secondary data allows the KB processor to exploit "what the radar is seeing".

This section presents a detailed description of the MAP-STAP [20]. Section 3.3.1 discusses the difficulty in choosing secondary data for estimation of a clutter covariance matrix in non-homogeneous clutter environments. This section concludes with an approach for easing this difficulty in adaptive post Doppler processing. Section 3.3.2 presents a description of our *a priori* data approach to estimate the clutter covariance matrix in non-homogeneous environments. Section 3.3.3 presents our stated research problem, hypothesis, and preliminary findings. Section 3.3.4 presents our conclusions and recommended future work.

### 3.3.1 Representative Secondary Clutter Data

Assume the test cell in which a target is to be detected is located in the  $l^{\text{th}}$  range ring as shown in Figure 33. Since  $R_l$ , the clutter covariance matrix of the  $l^{\text{th}}$  range ring is unknown, the objective is to select secondary data from other range rings in order to estimate  $R_l$ . Suppose attention is focused on the  $(l')^{\text{th}}$  range ring where  $l' \neq l$ . The question that arises is, "Is the clutter in the  $(l')^{\text{th}}$  range ring representative of the clutter in the  $l^{\text{th}}$  range ring?" This will be the case provided that to each clutter patch in the  $l^{\text{th}}$  range ring having a specific mean-square complex amplitude magnitude and a specific pair of normalized Doppler and spatial frequencies there is a corresponding clutter patch in the  $(l')^{\text{th}}$  range ring having approximately the same mean-square complex amplitude and approximately the same normalized Doppler and spatial frequencies.

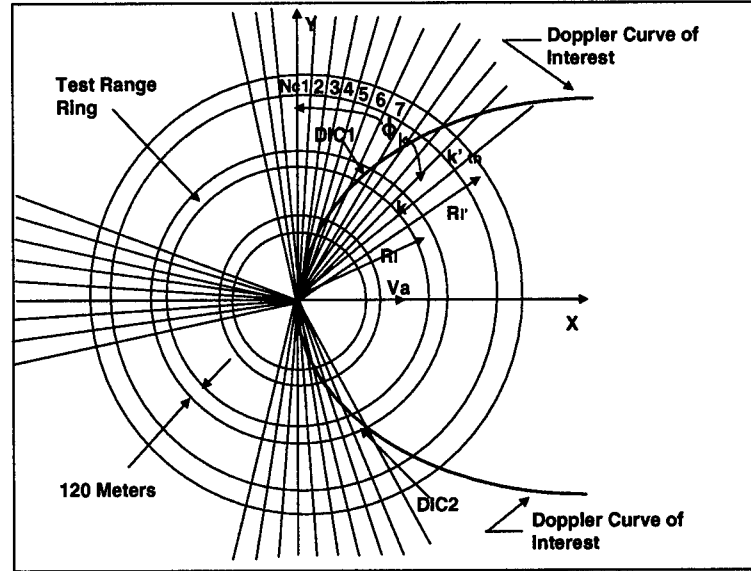


Figure 33: Range Ring and Doppler Patch Model with Constant Frequency Hyperbola

Consider the  $(k')^{\text{th}}$  clutter patch in the  $(l')^{\text{th}}$  range ring. The normalized Doppler and spatial frequencies associated with this clutter patch are

$$\begin{aligned}\bar{\omega}_{lk'} &= \frac{2v_a}{f_r \lambda_o} \cos \theta_{l'} \sin \phi_{k'}, \\ v_{lk'} &= \frac{d}{\lambda_o} \cos \theta_{l'} \sin \phi_{k'}.\end{aligned}\tag{31}$$

Let the normalized Doppler and spatial frequencies for a clutter patch equal  $\omega_o$  and  $v_o$ , respectively. Assuming a flat earth, the constant Doppler frequency contour for  $\omega_o$  is the hyperbola given by

$$\left[\left(\frac{2v_a}{f_r \lambda_o}\right)^2 - \bar{\omega}_o^2\right] x_c^2 - \bar{\omega}_o^2 y_c^2 = \bar{\omega}_o^2 h^2, \quad (32)$$

where  $h$  is the height of the airborne platform and  $(x_c, y_c)$  are the coordinates of the clutter point scatterer. Similarly, the constant spatial frequency contour for  $v_o$  is the hyperbola given by

$$\left[\left(\frac{d}{\lambda_o}\right)^2 - v_o^2\right] x_c^2 - v_o^2 y_c^2 = v_o^2 h^2. \quad (33)$$

Using the fact that  $\omega_o = (2v_a/f_r d) v_o$ , it can be shown that the hyperbola given by Eqn. (32) is identical to the hyperbola given by Eqn. (33).

Even though the pairs of normalized Doppler and spatial frequencies remain invariant from one range ring to another and even if clutter patches are identified such that  $\omega_{r'k} = \omega_{rk}$ , it is unlikely in a non-homogeneous clutter environment that  $E[|\alpha_{r'k}|^2] = E[|\alpha_{rk}|^2]$  for all  $N_c$  pairs of clutter patches in the two range rings. In fact, unless the clutter is entirely homogeneous in both range rings, the clutter in the  $(l')^{\text{th}}$  range ring will not be representative of the clutter in the  $l^{\text{th}}$  range ring over the entire clutter ridge.

The concept of representative secondary clutter data, however, may be meaningful on a selective basis. For example, consider post-Doppler adaptive beamforming in which nonadaptive Doppler filtering is first performed separately on the  $M$  pulses from each array element. In effect, this produces at each array element the output of  $M$  Doppler filters which subdivide the normalized Doppler frequency interval into  $M$  contiguous Doppler bins. For each of the  $M$  Doppler bins, adaptive spatial filtering is subsequently performed to reduce the residual clutter. Because the residual clutter in normalized Doppler and spatial frequencies is confined to a localized region along the clutter ridge, it is no longer necessary that the range ring from which secondary data is being collected be equivalent in its entirety to the primary range. Now the clutter in only a few patches of each range ring need be equivalent i.e. those that lie along the same Doppler ridge.

To assist us in building and testing our methodology for selecting equivalent range rings we are using data gathered under the MCARM program. We chose this data because of its varied and heterogeneous clutter environment.

### 3.3.2 A Priori Information

This section presents a detailed discussion of the use of *a priori* map data derived from US Government databases. We are assuming that the interference limiting a side looking airborne radar is due to ground and angel clutter. These reflections are due to static and dynamic objects. Dynamic objects move during an airborne radar's mission e.g. cars, buses, trucks, trains and flying objects such as aircraft, balloons, and birds. Static objects are the earth and man made objects on the earth that do not change rapidly

over time e.g. buildings, roads, power lines, and bridges. For this effort we are concerned with static objects and associated *a priori* data.

The results presented here focus on the MCARM database. Data has been obtained for the Delmarva Peninsula from the United States Geological Survey (USGS) and the National Imagery and Mapping Agency (NIMA). The USGS has three types of data that are of interest with varying levels of precision. The Land Use and Land Cover (LULC) data describe the earth based upon a classification system with 9 major codes and 38 minor codes. The Digital Line Graph (DLG) data describe the features of the earth by bounding them with polygons described by curved or straight lines. There are 305 features. The NIMA databases are similar to the USGS except they provide more precise and more detailed data than the USGS. We have written software to translate these data, defined a database schema for both, loaded their data within a relational Database Management System (DBMS), and written software that registers the beam patterns of the MCARM radar upon the earth. Given the results of this work one can now query and render their data in 2-D and 3-D depicting them in a virtual reality world using a Beta version of Virtual Reality Modeling Language (VRML). The user "sees what the sensor is seeing".

The approach we have taken is to classify each of the patches on the earth within the surveillance volume. Those patches that lie along the Doppler of interest and have the same classification as DIC1 (Figure 33) are candidate rings for secondary data.

There are different data sources available for classifying the contents of patches. Since the Delmarva Peninsula is relatively flat (within a 500 square mile area the elevation varies less than 90 meters), we did not include DEM data and we focused on LULC data. The LULC data we are concerned with are the latitude (lat) and longitude (lon) for points on the earth and their LULC codes. The data file we used provides this data for each 200x200m area. Note that the range resolution of our MCARM radar is 120 meters! For our algorithm, patches that have the same major code are considered equivalent, even though one may have a road in it and one may not, or one may contain streams and the other a lake.

### **3.3.3 Research Problem, Hypothesis, and Preliminary Findings**

To determine if post Doppler STAP performance can be improved upon by choosing secondary data locations from maps, we compare our results with the standard sliding window approach. The sliding window algorithm chooses the first  $K/2$  range rings further than the test ring and the first  $K/2$  range rings from the test ring and closer to the radar, minus the two range rings next to the test range ring. ( $K$  is twice the number of independent channels of the MCARM radar i.e. 44.) See Figure 17(a). The sliding window algorithm has an implicit assumption that the nearby range rings of the test ring are homogeneous and are representative of the test ring. Based on the registration of the

**MCARM Acquisition Plot**

**LULC**  
Land Use Land Coverage

- ☒ Agricultural
- ☒ Barren
- ☒ Forest
- ☒ Rangeland
- ☐ Snow
- ☐ Tundra
- ☒ Unknown
- ☒ Urban
- ☒ Water
- ☒ Wetland

**DLG**  
Digital Line Graph

- ☐ Misc
- ☐ Railroads
- ☐ Roads

**Radar Features**

- ☒ Range Bins
- ☒ Angle Bins
- ☒ Doppler Bins
- ☒ Plane Data

**Start Ang Bin**  
10

**End Ang Bin**  
100

**Ang Bin Int**  
1

**Start Rng Bin**  
100

**End Rng Bin**  
600

**Rng Bin Int**  
50

**Range Bin**  
600

**Angle Bin**  
54

**Doppler Bin**  
17

**Lon**  
-75.41887

**Lat**  
39.983826

**Reset** **Render** **Exit**

56

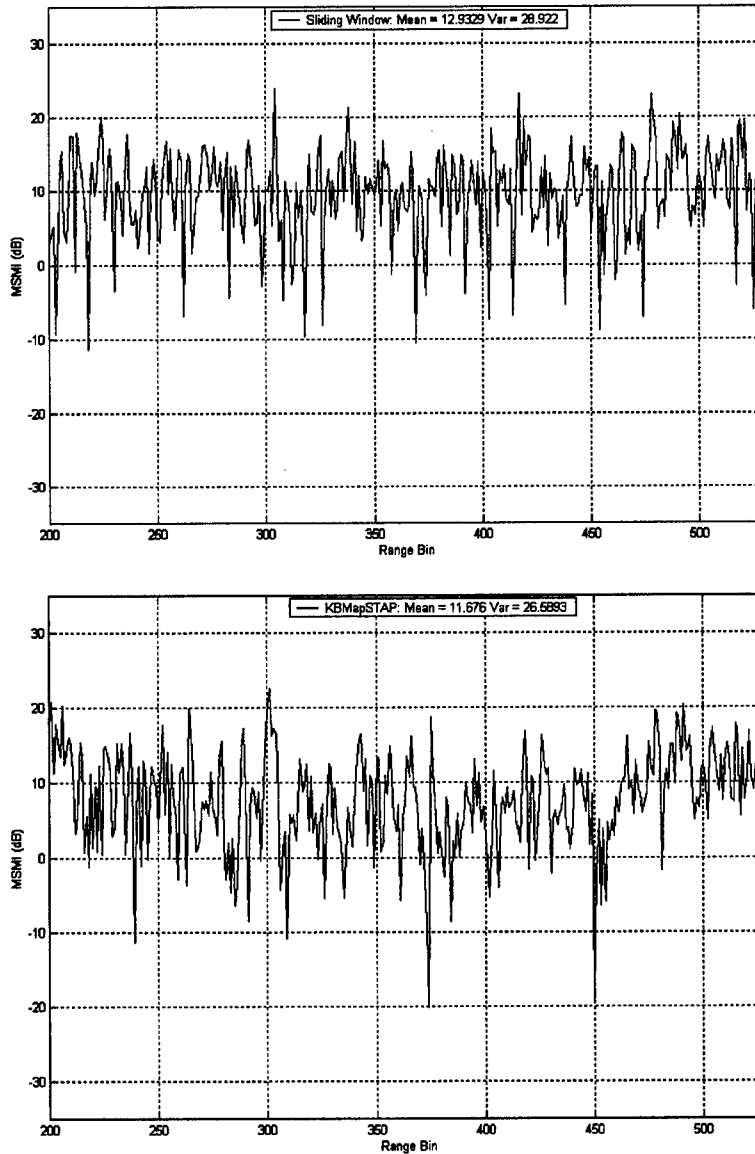


**Figure 35: MSMI Output With No Injected Target**  
**(a) Using Sliding Window Algorithm (b) MAP STAP Algorithm**

It was our hypothesis that MAP STAP would do as well as the sliding window algorithm in homogeneous environments and would do better than the sliding window approach for areas where the ground is heterogeneous. To test our hypothesis, a target was injected at different range rings with the same radial velocity of 31m/s (i.e. Doppler bin 17). The only difference in the implementation of the two algorithms was in the choice of the secondary data. Preliminary results, using the Modified Sample Matrix Inversion (MSMI) algorithm, are shown below. The MSMI statistic, which has an embedded CFAR property [7], is computed for each range ring of interest after Doppler processing.

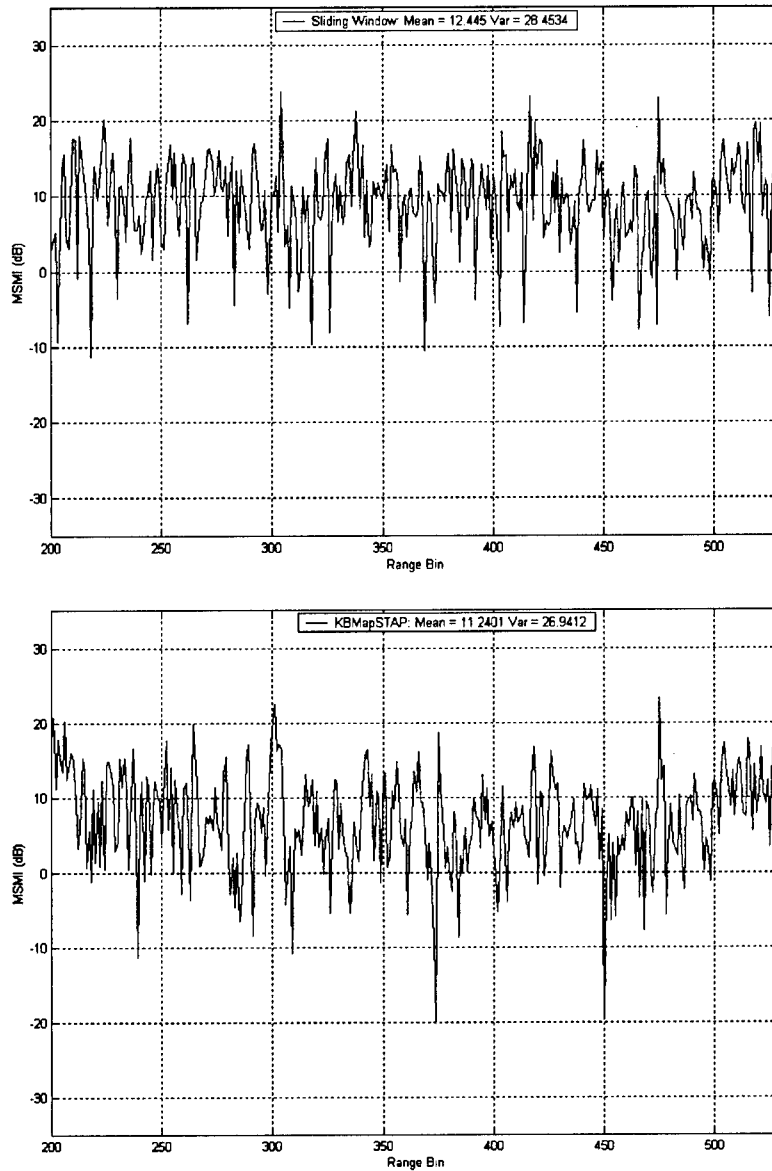


**Figure 36: MSMI Output With Injected Target at Range Bin 475  
(a) Using Sliding Window Algorithm (b) MAP STAP Algorithm**

Figure 35 represents the MSMI for the two algorithms without an injected target. The mean and variance of the results are slightly smaller for MAP STAP than for the sliding window algorithm. If a threshold of 20 db were chosen, then the MAP STAP would detect fewer false alarms than the sliding window algorithm.

To test our hypothesis that the MAP STAP algorithm would perform the same as the standard algorithm when a target occurred in a homogeneous clutter environment, we injected a target in range bin 475. Figure 36 shows the result of the sliding window algorithm and for MAP STAP. It was conjectured that MAP STAP would do as well as the sliding window algorithm and it did.



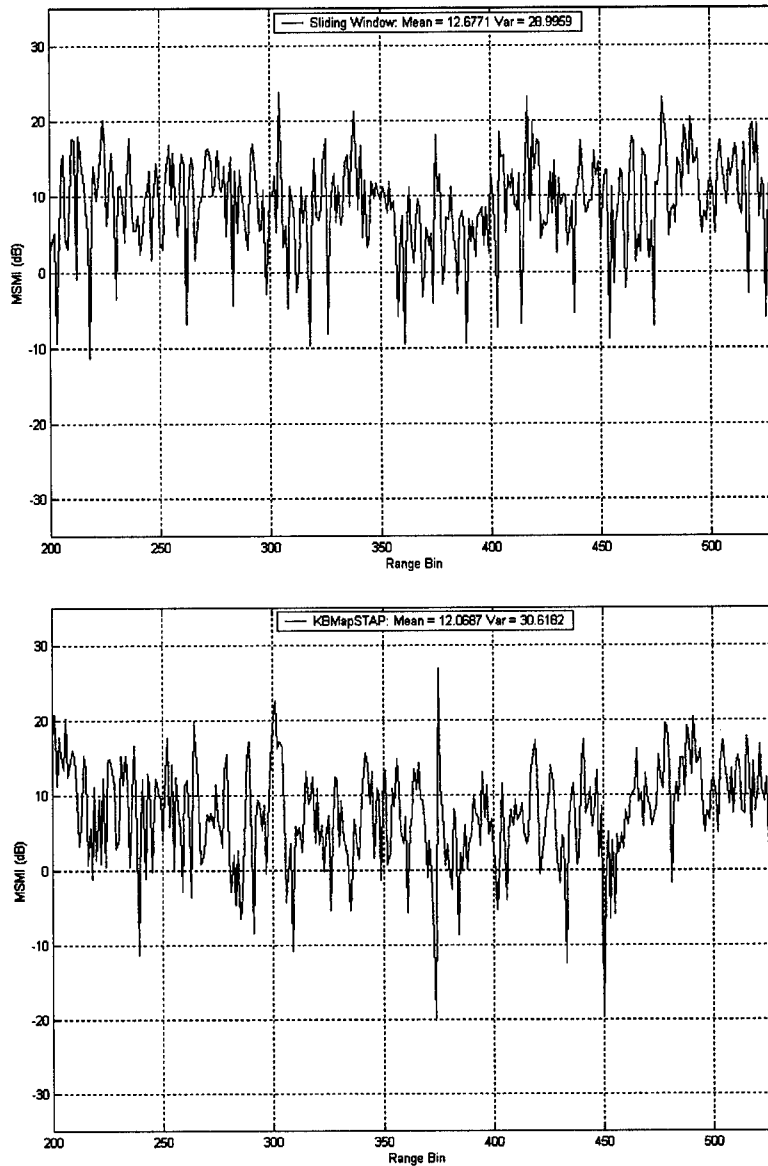


**Figure 37: MSMI Output With Injected Target At Range Bin 375**  
**(a) Using Sliding Window Algorithm (b) Using MAP STAP**

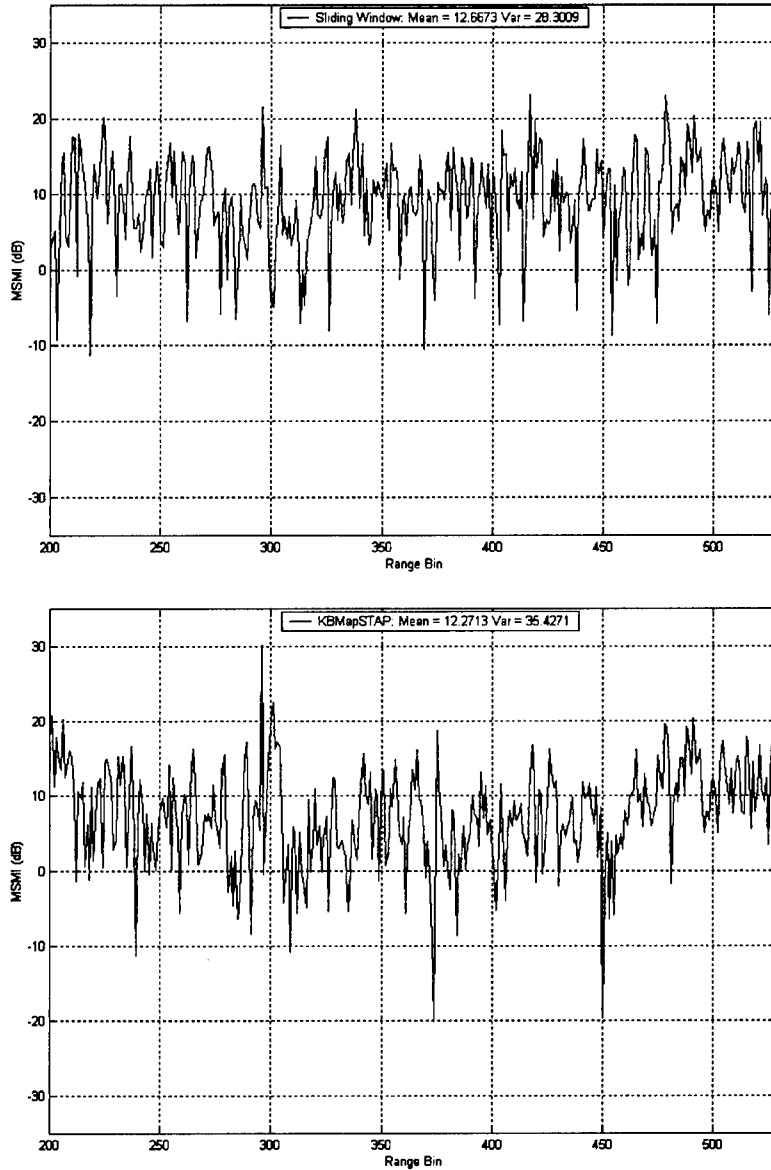


**Figure 38: MSMI Output With Injected Target At Range Bin 296**  
**(a) Using Sliding Window Algorithm (b) Using MAP STAP**

Figure 37 has the injected target in range bin 375 where the surrounding range rings are relatively heterogeneous. Figure 37(a) shows the result of the standard algorithm and Figure 37(b) the result for MAP STAP. It was conjectured that the MAP STAP would do better than the sliding window algorithm and it did. The same is shown in Figure 38 where the injected target is in range bin 296. In these two cases, MAP STAP yields fewer false alarms.

### 3.3.4 Discussion

Major issues still need to be explored. The data from the USGS database were collected approximately 10 years before the radar data were obtained. It is likely that some of the USGS data was not current when the radar data were collected.

Map precision is also important when the range and angle resolution is significantly different from that of the map data. For our experiments radar range was 120 meters and the LULC data points were every 200 meters by 200 meters. Even with this difference in precision the MAP STAP algorithm performed well. The Delmarva area is relatively flat and using LULC data worked well. If however, the terrain is mountainous then the algorithm must include digital elevation model data

## 4.0 GMTI-STAP Future Work

Sections 2.0 and 3.0 have presented past and on-going research on the transition of space-time adaptive processing from theory to practice. In particular, concepts including spatial DOF reduction, array effects, non-homogeneous data were presented, finally leading to the KB-STAP concept. Research on MAP-STAP significantly enhances KB-STAP, using *a priori* map data to inform the knowledge base. The adaptive processing concepts developed were applied to AMTI and GMTI.

This section presents proposed future work in the GMTI specific application. GMTI requires that additional attention be paid to the specific problem of low target velocity, with the target signal competing with mainbeam clutter.

### 4.1 $D^3 \Sigma \Delta$ STAP

This near-term task will develop and evaluate a specific algorithm designed to address both the clutter non-homogeneity and slow velocity issues. STAP has long been known to have hard-to-predict spatial response patterns including very high sidelobes in some interference-free regions, loss of mainlobe gain, and significantly shifted mainlobe gain. These mainlobe impacts will be of much greater importance when addressing the slower targets of the GMTI task and thus must be minimized. The high sidelobes in regions that are evaluated by the secondary data to be interference free will make the algorithm sensitive to even small clutter non-homogeneities. The excellent performance of the  $\Sigma \Delta$  algorithm resulted from the low sidelobe of the sum and difference beam systems and the low gain of the difference beam in the direction of the target. These factors give the  $\Sigma \Delta$  algorithm a more predictable response pattern.

The work proposed for the near term will be an attempt to combine the advantages of the previous hybrid STAP algorithm (Section 3.1) and the  $\Sigma \Delta$  STAP algorithm (Section 4.1) to better address non-homogeneous clutter. In addition the delta channels will be

chosen to minimize the impact of the adaptive process on the target return, that is, the low velocity issues.

The previous hybrid STAP algorithm employed a direct data domain ( $D^3$ ) algorithm for the first stage to suppress discrete non-homogeneities in the range cell under test. This algorithm served as an adaptive transformation from the space-time domain to the angle-Doppler domain and was followed by a statistical STAP algorithm to filter residual correlated interference. The  $D^3$  algorithm constrained the antenna gain in the direction of the target in angle and Doppler space. If the target is not exactly at the center of the antenna mainbeam the target return can be attenuated by this  $D^3$  process. A version of the  $D^3$  algorithm has been developed which maximizes the antenna gain across the antenna mainbeam to overcome this attenuation [21].

In this new algorithm a  $D^3$  process will be developed to constrain both a sum beam and a difference beam across the transmit mainbeam and to use these sum and difference beams as the first stage of a hybrid algorithm with a statistical algorithm as the second stage. Multiple delta beams pointing in different angles within the sum beam will be investigated.

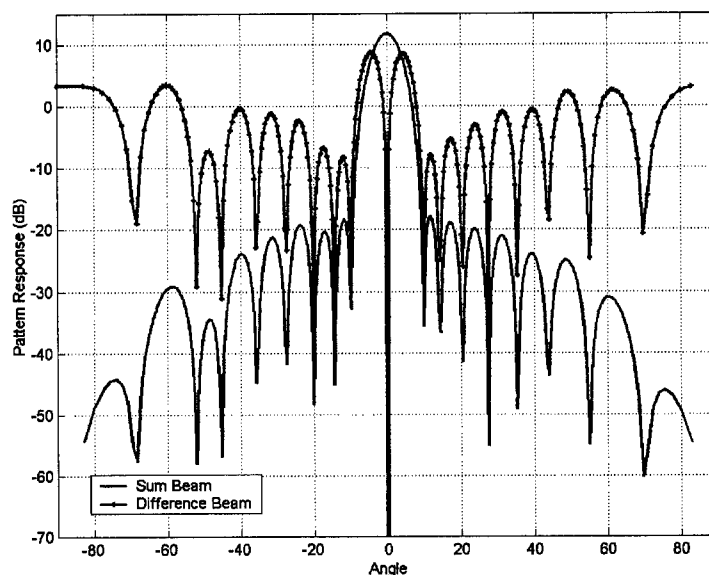


**Figure 39: Sum and Difference  $D^3$  Beam Patterns**

The work of developing a rigorous formulation in evaluating these beams has only just begun. Figure 39 illustrates the results of a simple formulation extending the hybrid formulation to the  $\Sigma\Delta$  case. The example presented uses 18 elements and 18 pulses in the CPI. An artificial non-homogeneity is injected at angle bin  $-51^\circ$ , while the look angle is maintained at  $0^\circ$ . As can be seen, both the sum and difference channels place a null in the direction of the discrete interference, while maintaining the desired response at the look angle. The sum channel places maximal gain in the look direction, while the difference (delta) channel places a null at the look direction.

The results shown in Figure 39 are preliminary, but show the promise of investigating a  $D^3 \Sigma \Delta$  STAP formulation. The work of formalizing the process of obtaining these sum and difference weights is on going and will continue in the near future.

In the longer term, this  $D^3 \Sigma \Delta$  algorithm can be improved by incorporating two concepts: first, MAP-STAP can be used to determine the best data samples to be used for statistical processing in the second stage. Second, the location of the mainbeam clutter ridge is determined *a priori* by the motion of the aircraft platform. This information can be exploited by using a *constrained*  $D^3$  algorithm which places a null (in the Doppler domain) at this mainbeam clutter location. This approach should improve the ability of the  $D^3$  algorithm to suppress correlated mainbeam clutter.

## 4.2 Additional Algorithms

The major difference between GMTI adaptive filtering algorithm and the existing AMTI adaptive filtering work is that the clutter competing with the target is coming from angles that are in the antenna mainbeam or near-in sidelobes whereas AMTI clutter is at angles in farther out sidelobes. Thus the potential for significant impact on the target return is greater for GMTI than it was for AMTI. The focus of filtering algorithm development will be on algorithms that minimize that effect. Additional effort on hybrid algorithms with new versions of the  $D^3$  algorithm for the first stage is planned.

Knowledge-based (KB) processing has been shown to improve both the filtering and detection stages of radar signal processing. In both cases the KB part of the processing is accomplishing similar functions: selection of optimum algorithm and selection of secondary data for the algorithm chosen. The integration of KB processing for the two stages including feedback from detection to filtering has potential for additional improvement in overall performance. Integrated KB adaptive filtering and detection/CFAR will be developed in future efforts.

### 4.2.1 Evolutionary Algorithms

The selection of the best STAP algorithm for a particular real-world environment is difficult because of the large number of possibilities and because the environment does not satisfy the independent and identical distribution condition that would make theoretical solution of the problem possible. Knowledge-based approaches that address the actual environment have been shown to perform better than theoretically optimum algorithms in these real-world environments. But these KB approaches can not be analyzed from basic principles and there are so many possibilities that comparison of all of them appears difficult.

Expert system and knowledge-based technology has also been shown to have significant payoff for the other steps in radar signal processing (detection/CFAR, tracking) in these same real-world environments [18]. Each step in the signal processing has been

investigated separately and the algorithms tested for performance at that phase. Since there are dependencies between the performance in step of the processing of the previous steps, it seems reasonable that integrated KB processing with feedback between stages could have better performance than algorithms developed for each step separately. Integrated end-to-end signal processing will have a much greater number of algorithm options because more filtering algorithms can be combined with most detection algorithms and those combinations can be combined with most tracking algorithms.

## 5.0 Roadmap to the Future

AFRL has produced a plan to develop and transition the technology and sensor/platform concepts for the cost-effective surveillance for future GMTI threats in all environments. Based on the technology of the DARPA/AFRL program the three-phase program will investigate the surveillance of both slower and smaller targets in all clutter and countermeasure environments. The focus of the program will be on accomplishing the mission on smaller and less expensive platforms.

Adaptive processing algorithms will be developed to obtain the lowest MDV possible for a given size antenna, while improving accuracy and classification performance. This adaptive capability will address the real interference environment including clutter from all regions of the world including the severe non-homogeneous clutter of urban areas and various jammer types including high power noise, 'hot clutter' and deceptive jammers.

The plan is divided into three programs (Figure 40): technology, maturation (transition from the technologist to the developer) and demonstration (transition from the developer to the user).

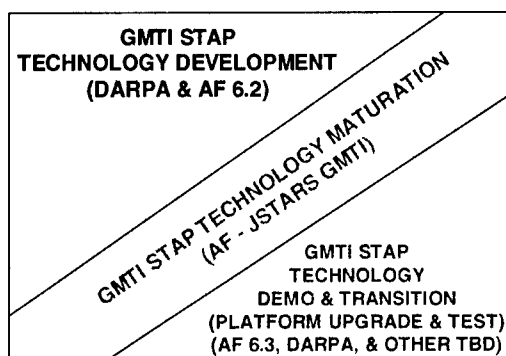
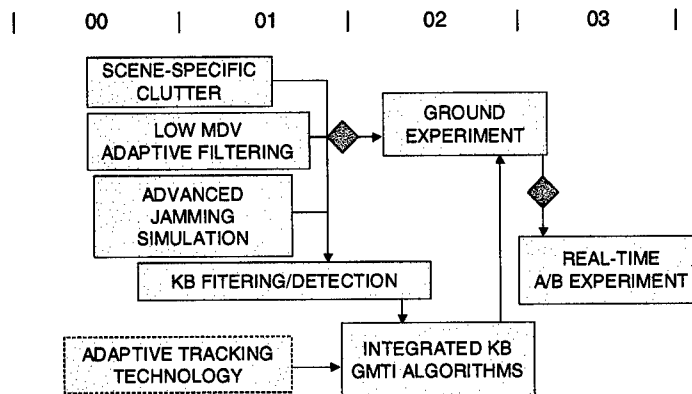


Figure 40: GMTI STAP Plan

A roadmap for the technology program is shown in Figure 41. During the first two years the technology will focus on GMTI-specific STAP algorithm development, the modification of an existing high-fidelity simulation to address specific GMTI issues and employment of that simulation to verify the performance of the new algorithms. This two-year technology development effort forms the foundation for continued collaboration with the developer and the user. The new STAP filtering algorithms will be integrated with advanced detection algorithms to improve overall target detection performance. In the

third year of this program ground experiments will be performed using existing AFRL facilities to validate algorithm performance and the advanced filtering and detection algorithms will be integrated. This integration will use the knowledge-based control to optimize all phases of the processing. In the fourth year the integrated algorithms will be demonstrated with airborne measurements. Decision points are envisioned before major-cost efforts of ground based and airborne testing.



**Figure 41: Technology Program Roadmap**

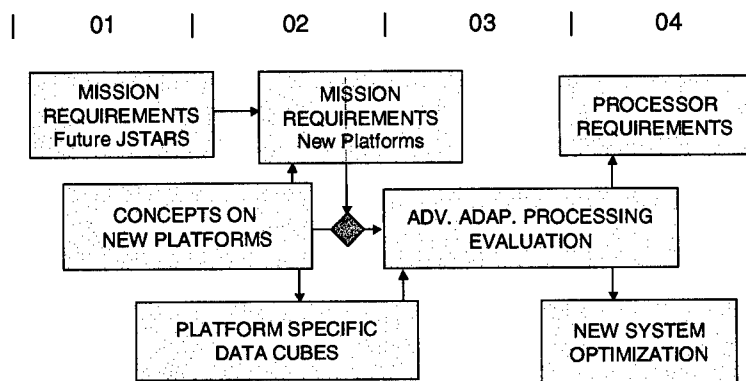


**Figure 42: Technology Maturation Program Roadmap**

The maturation program (Figure 42) will define the new mission requirements, develop sensor concepts on various low-cost platforms, evaluate the adaptive processing algorithms, define processor requirements and develop design techniques for modular radar. The demonstration program will use an airborne demonstration on a smaller and less expensive platform to validate the modular sensor and advanced processing technologies. Possible platforms include UAV's, including Global Hawk and smaller UAV's, and business jets. The three-phase plan (Figure 42 and Figure 43) is integrated with decision points at which the parallel progress of the programs can be evaluated and with feedback between the three programs. Decision point one will evaluate the progress

of the technology. Its exit criteria will be (i) GMTI algorithms developed that provide significant performance improvement and (ii) algorithm performance validation by computer simulation. Decision point two will evaluate the progress of the technology and the maturation efforts. Its exit criteria will be (i) validation of algorithm performance by ground experiments and (ii) the development of new GMTI concepts with significant cost savings predicted.

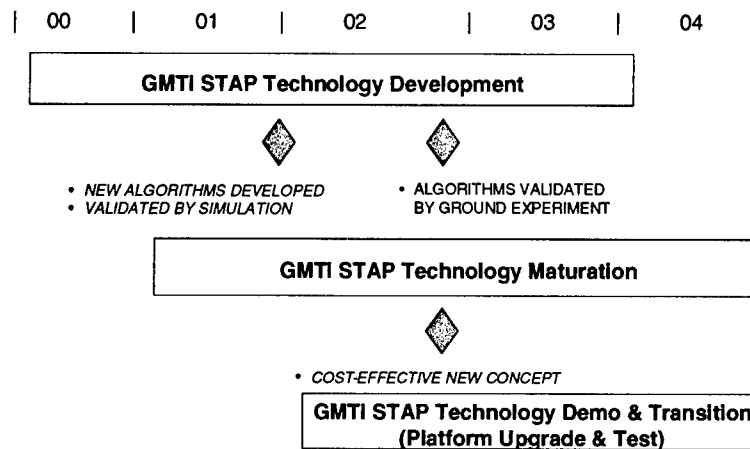


**Figure 43: GMTI STAP Program Roadmap**



## 6.0 References

- [1] M.C. Wicks, *A Comparative Study of Space-Time Processing for Airborne Radar*, Ph.D. Thesis, Syracuse University, May 1995.
- [2] I.S. Reed, J. Mallet, and L. Brennan, "Rapid convergence rate in adaptive arrays", *IEEE Trans. on AES*, vol. 10, no. 6, pp. 853-963, December 1974.
- [3] H. Wang, "Space-Time Adaptive Processing for Airborne Radar", in *Digital Signal Processing Handbook*, V. Madisetti and D. Williams eds., CRC Press 1997.
- [4] S.M. Sherman, *Monopulse Principles and Techniques*, Artech House, 1984.
- [5] J. Maher, Y. Zhang and H. Wang, "Space-Time Adaptive Processing with Sum and Difference Beams for Airborne Radars," *Proc. SPIE's 13<sup>th</sup> Annual International Symposium on AeroSense*, vol. 3704, pp. 160-169, Orlando, FL, April 1999.
- [6] R.D. Brown, R.A. Schneible, H. Wang, M.C. Wicks, Y. Zhang "STAP for Clutter Suppression with Sum and Difference Beams", *IEEE Trans. on AESS*, April 2000.
- [7] H. Wang and L. Cai, "On adaptive spatial-temporal processing for airborne surveillance radar systems", *IEEE Transactions on AES*, vol. 30, No. 3, pp. 660-669, July 1994.
- [8] J. Ward, "Space-time adaptive processing for airborne radar", *Tech.Rep. F19628-95-C-0002*, MIT Lincoln Laboratory, December 1994.
- [9] R.S. Adve, T.B. Hale and M.C. Wicks, "Joint Domain Localized Adaptive Processing in Homogeneous and Non-homogeneous Environments. Part I: Homogeneous Environments", *To appear in IEEE Proc. on Radar, Sonar and Navigation*. Accepted for publication November 1999.
- [10] W.L. Melvin and B. Himed "Comparative analysis of space-time adaptive algorithms with measured airborne data", *In Proceedings of the 7<sup>th</sup> International Conf. on Signal Processing Applications & Technology*, Boston, MA, October 1996.
- [11] D.K. Fenner and W.F. Hoover Jr., "Test Results of a Space Time Adaptive Processing System for Airborne Early Warning Radar", *Proc. IEEE National Radar Conference*, pp. 88-93, Ann Arbor, MI, May 1996.
- [12] "Multi-Channel Airborne Radar Measurements (MCARM) Final Report", vol. 1 of 4, *MCARM Flight Test*, Contract F30602-92-C-0161, for Rome Laboratory/USAF, by Westinghouse Electronic Systems.
- [13] H.H. Chang, "Improving Space-Time Adaptive Processing (STAP) Performance in Nonhomogeneous Clutter", *Ph.D. thesis*, Syracuse University, August 1997.
- [14] T.K. Sarkar and N. Sangruji, "An Adaptive Nulling System for a narrow band signal with a Look Direction Constraint Utilizing the Conjugate Gradient method", *IEEE Trans. on AP*, vol. 37, no. 7, pp. 940-944, July 1989.

- [15] R.S. Adve, T.B. Hale and M.C. Wicks, "Joint Domain Localized Adaptive Processing in Homogeneous and Non-homogeneous Environments. Part II: Non-Homogeneous Environments", To appear in IEE Proc. on Radar, Sonar and Navigation. Accepted for publication December 1999.
- [16] J.S. Goldstein, J.R. Guerci, I.S. Reed, "Advanced Concepts in STAP", Proc of 2000 IEEE International Radar Conference, Washington, DC, pp.699-704, May 2000.
- [17] J.R. Guerci, J.S. Goldstein, P.A. Zulch, I.S. Reed, "Optimal Reduced-Rank 3D STAP for Joint Hot and Cold Clutter Mitigation", Proc. of the 1999 IEEE National Radar Conference, Boston, MA, pp. 119-124, April 1999.
- [18] P. Antonik, H. Shuman, P. Li, W. Melvin, M. Wicks, "Knowledge-based Space-Time Adaptive Processing", Proc. of the 1997 IEEE National Radar Conference, Syracuse, NY, May 1997.
- [19] R.S. Adve, T.B. Hale, M.C. Wicks, P. Antonik, "Ground Moving Target Indication Using Knowledge Based Space Time Adaptive Processing", Proc of 2000 IEEE International Radar Conference, Washington, DC, pp.735-740, May 2000.
- [20] G. T. Capraro, C. T. Capraro, and D. D. Weiner, "Knowledge Based Map Space Time Adaptive Processing (KMapSTAP)", AFRL-SN - unpublished final report.
- [21] R. Schneible, "A Deterministic Least Squares Approach to STAP", Ph.D. thesis, Syracuse University, May 1996.